MSUCL-44

Energy Dependence of Proton Inelastic Scattering from ^{40}Ca †

C.R. Gruhn,†† T.Y.T. Kuo,††† C.J. Maggiore,* H. McManus,
F. Petrovich,** and B. M. Preedom***

Department of Physics and Cyclotron Laboratory
Michigan State University
East Lansing, Michigan 48823

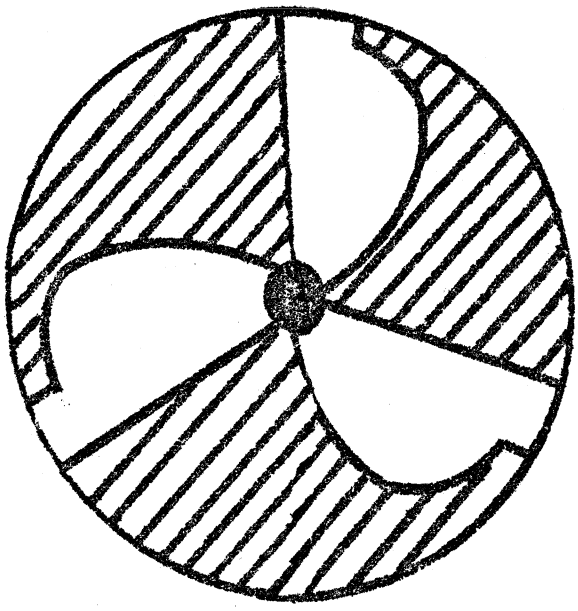

CYCLOTRON LABORATORY
MICHIGAN STATE UNIVERSITY

*SUPPORTED BY THE U.S. NATIONAL SCIENCE FOUNDATION

Energy Dependence of Proton Inelastic Scattering from ^{40}Ca[†]

C.R. Gruhn,[††] T.Y.T. Kuo,[†††] C.J. Maggiore,[*] H. McManus, F. Petrovich,[**] and B.M. Preedom[***]

Department of Physics and Cyclotron Laboratory
Michigan State University
East Lansing, Michigan 48823

---

† Supported in part by the National Science Foundation.

†† On sabbatical leave to CERN, Genève, Switzerland.

††† Submitted in partial requirement for Ph.D.

Present Address: Department of Physics, Sloan-Kettering Institute, New York, New York

* Present Address: Department of Environmental Medicine, Mt. Sinai School of Medicine, New York, New York

** Present Address: Lawrence Radiation Laboratory, University of California, Berkeley, California 94720

*** Present Address: Physics Department University of South Carolina, Columbia, South Carolina 29208

ABSTRACT

Inelastic proton scattering from ^{40}Ca has been measured at beam energies of 24.93, 30.04, 34.78, and 39.83 MeV. Angular distributions from 13° to 97° for about 40 inelastic states were obtained. Analyses with both microscopic and macroscopic theories are presented.

INTRODUCTION

The doubly magic nuclei, such as ^{40}Ca, have been studied in great detail both experimentally and theoretically. The degree of deviation from a simple double closed shell structure is of great interest. Recent advances in the theories of nuclear shell-models (RPA and deformed), the effective nucleon-nucleon force, and the distorted wave treatment of direct reaction enable one to formulate a microscopic description of the inelastic scattering of protons by nuclei.[1-6] The ^{40}Ca nucleus was chosen as a target to test the (p,p') reaction as a probe of nuclear structure because of the following points. First, it is a target which allows the (p,p') reaction to examine all the components of the proton-nucleus force. Second, it is a target in which the eigen-vectors describing the excited states are relatively well established both experimentally and theoretically. Third, it is a target for which good optical model parameters exist.

The structure of ^{40}Ca has also been investigated in other experiments such as (α,α'),[7,8] (e,e'),[9,10] (^{3}He,d),[11] (d,n),[12] and $(p,p'\gamma)$.[13] The (α,α') reaction is a predominantly surface-dominated reaction and it leads to diffraction scattering. It measures L-transfer for the excited normal-parity states, and the isoscalar component of the projectile-nucleon force. The (e,e') reaction gives reduced electromagnetic transition

probabilities and multipolarities. The (^{3}He,d) and (d,n) proton stripping reactions allow one to study individual components of the vectors of the excited states. The (p,p'γ) reactions have been used primarily to determine the spins and parities of the excited states. Whereas the (p,p') reaction is useful in probing various components of the effective interaction and testing microscopic wave function.

By studying the energy dependence of the reaction, in many cases, one is able to remove ambiguities due to reaction mechanism problems. The present experiment studies proton inelastic scattering from ^{40}Ca at bombarding energies of 24.93, 30.04, 34.78, and 39.83 MeV. Spectra were taken simultaneously by two surface barrier Ge(Li) detectors with an overall resolution of 30-keV (FWHM). Angular distributions for inelastic scattering to approximately 50 excited states were obtained over the angular range from 13° to 97° (LAB). The data were analyzed using both a collective model to extract L-transfers and nuclear deformations and a microscopic model employing a realistic force, RPA wave functions, and approximate exchange.

II. EXPERIMENTAL APPARATUS AND PROCEDURES

The data were obtained using protons from the Michigan State University sector-focused cyclotron.[14-16] The beam was energy-analyzed using two 45° bending magnets with

image and object slits set to pass beam with fractional energy spread of $\pm 1.25 \times 10^{-4}$. Detailed discussions of the optical properties of the beam and of the energy analysis system are given elsewhere.[17-19] The absolute energies of the proton beams were obtained from NMR calibrations of the magnets. The uncertainty in this absolute scale was $\pm 0.1\%$.[17] The absolute beam energies for this experiment were 24.93 ± 0.03 MeV, 30.04 ± 0.03 MeV, 34.78 ± 0.04 MeV, and 39.83 ± 0.04 MeV.

The beam on the target was monitored using both a Faraday cup and a Ge(Li) proton detector placed at 45 degrees with respect to the beam. The scattering chamber[20] used in this experiment consisted of a target chamber which was viewed through ports in a sliding seal. Two ports separated by 14.7° were coupled such that a pair of Ge(Li) protons detectors could be used. The solid angles of the two detectors were $1.38 \pm 0.04 \times 10^{-4}$ sr and $0.786 \pm 0.024 \times 10^{-4}$ sr for detectors 1 and 2 respectively. The angular range of detection was from 12° to 97° in 5° steps. Data were taken twice at 27° and 72° by each detector for the relative normalization . Details concerning these detectors are given in a previous publication.[21] The target was a rolled, self-supported 2 mg/cm^2 foil of enriched (99.973%) ^{40}Ca. The isotopic and spectroscopic analysis supplied by ORNL is listed in Table I.

Dead-time corrections were made for all spectra including those taken by the monitor counter. The dead-times for most spectra were under 2%. For only a very few cases (5 out of 100) in which the detector was set at a small angle, were corrections found to exceed 5%, the largest being 12%.

Representative spectra are shown in Fig. 1 to Fig. 4. In the group of elastic peaks two small ones can be seen, one of which is from high Z contaminants and the other was identified as ^{19}F. States up to 10.3 MeV excitation energy were observed. The broad peak at high excitation energy was due to a tantalum degrader slit used as a collimator in front of the Ge(Li) detector. The ground state of the $^{40}Ca(p,d)$ reaction having a Q-value of -13.863 MeV was also observed.

The overall resolution was about 30 keV (FWHM). The sources and their contributions to the energy resolution are tabulated in Table II for 40-MeV protons.

Angle Calibration

The laboratory angle for each spectrum was determined by the energy separations between the elastic peaks of ^{40}Ca, ^{16}O, and ^{12}C and the 3^- excited state of ^{40}Ca at 3.736 MeV. The experimental energies of these peaks were calculated from the positions of their centroids. With the known energy difference between the ^{40}Ca [0.000 MeV] and the $^{40}Ca^*$ [3.736 MeV] states

at a particular angle, the energy spacing between these four peaks were computed. However, without knowing the exact angle, the energy calculation is only approximate. It was necessary to reiterate this angle and energy calibration procedure. Most computations required only two iterations since the energy difference between the $^{40}Ca^{*}$ [3.736 MeV] and ^{40}Ca [0.000 MeV] states changes slowly with respect to angle (about 0.8 keV/deg. at 25° and 1.7 keV/deg. at 100°).

For laboratory angles less than 28°, the H(p,p)H reaction was also used. The fact that the kinematics of this reaction is strongly dependent on angle provided an acute test of the accuracy of the method described above. The agreement between these two calibration methods was within 0.04 degree.

The effect of the uncertainties in the beam energy and in the centroids of peaks upon the accuracy of determinations of the laboratory angle was studied. Two kinematics calculations were done using E_p=35.000 MeV and 34.775 MeV. The laboratory angles calibrated by these two calculations agreed to within 0.1 degree. When the centroids were allowed to fluctuate $\pm$0.2%, the calibrated angles varied by $\pm$0.04 degree. We conclude that our angle calibration error is less than $\pm$0.05 degrees.

Absolute Cross Sections

The detector, monitor, and Faraday cup system were calibrated using proton scattering from the hydrogen contained in a clear

mylar target. The cross section for this reaction is known to $\pm$.5% at these energies.[22] As a check of this calibration procedure, differential cross sections were measured for elastic proton scattering from ^{12}C, ^{16}O, and ^{40}Ca. A comparison of these measurements with those of other references is given in Table III. The errors given for this experiment in Table III are statistical only.

A detector efficiency of 0.9875[23] was assumed for these measurements. If one uses these additional measurements as a part of the cross section calibration, an error of $\pm$3% can be assigned to our cross section measurements.

Treatment of Data from Contaminant Nuclei

The main contaminants observed were ^{1}H, ^{12}C, and ^{16}O. The hydrogen and carbon came from the deposition of pumping oil on the target while the oxygen came from the oxidation of the Ca during the mounting of the target foil the contamination of spectra due to peaks in the response function of Ge(Li) detector is ruled out by inspection of the spectra.

A complete analysis was made for ^{12}C and ^{16}O states. A mylar target was used to measure the ratio of counts of the inelastic to the elastic peaks at the identical angles at which ^{40}Ca data were taken. This method provided a reference to monitor the intensity of the contaminant peaks in the ^{40}Ca

spectra. Once the ratio of counts in the mylar run was computed, the number of counts for the same inelastic contaminant peak in a ^{40}Ca spectrum was easily determined as long as the elastic counts were known.

The corrections for contaminants at small angles, where the ^{12}C and ^{16}O elastic peaks could not be separated from that of ^{40}Ca, required a measurement of the amount of each contaminant in the target. The angular distribution of relative cross sections in the laboratory system for the ^{16}O elastic peak was first obtained. This result was compared with the measurement reported by Cameron.[24] Good agreement in the shape of the distribution was noted. This suggested that the amount of ^{16}O on the target remained essentially constant in the course of the whole experiment. Secondly, the amount of ^{16}O in the target was calculated by using Cameron's data. Several values were computed over a few angles around $\theta_{LAB}=50°$ where the distribution is flat. The average value of the amount of ^{16}O in the ^{40}Ca target used was found to be 0.0192 ± 0.002 mg/cm^2. Similarly, the thickness of ^{12}C was measured to be 0.00258 ± 0.0003 mg/cm^2. his method allowed a correction at each energy to be made to that data in which the contaminant was not resolved from the state in ^{40}Ca.

The angular distributions of the differential cross sections for elastic scattering in the center of mass system are shown in Fig. 5.

The Decomposition of Multiplets

On the basis of Grace and Poletti's spectrum,[25] we know that several pairs of doublets with $\leq$20 keV separation were seen as single peaks in our spectra. Individual distributions could not be extracted directly from spectra for these states. It was decided that the angular distribution for the composite peak be analyzed first. Then, decomposition was done whenever it was possible.

Figure 6 illustrates the decomposition of the doublet at 8.564 MeV. The L-transfers to the component states were tentatively determined by examining the overall shape of the combined distribution. In this case they are L=5 and L=2. The shapes of the experimental angular distributions of the $4.917(5^-)$ and the $3.903(2^+)$ states were used in the decomposition and the ratio of cross sections was obtained by finding the best fit to all distributions at four energies. These fits are shown in Fig. 6.

In additon to the criterion of being a good fit for all four beam energies, the difference in differential cross section at various angles must also be consistent with the change of peak shape and centroid from one spectrum to another. It was found that the change of peak shape for this multiplet agreed with the above analysis. This also provided a way to determine the association of the spin and the excitation energy of the component states. The differential cross sections so obtained are estimated to be accurate to 30%.

Similar analyses were applied to the doublets at 7.543 and 8.100 MeV. The results are shown in Fig. 7 and 8. For the composite peak at 7.543 MeV, a fit was obtained by using the experimental distributions from the 3^- (3.736 MeV) and the 4^+ (6.505 MeV) states. Because of the similarity of L=3 and L=4 angular distributions, this assignment of spins is considered to be highly questionable.

The components of the 8.100 MeV doublet were assigned L=2 and L=3. It should be noted that the experimental angular distribution for the 6.285 MeV state, instead of that for the 3.733 MeV state, was used for the L=3 distribution to obtain the best overall fit.

Grace and Poletti observed a triplet with excitation energies at 6.909, 6.930, and 6.948 MeV. The 6.930 MeV level was seen to be the strongest among this triplet in their spectrum taken at 87.5° at E_p=13.065 MeV. As shown in Fig. 9, the first and third members of this triplet were quite well resolved at smaller angles while the middle one was not seen. The solid line is drawn using a well resolved peak to give a representative "standard" singlet peak.

At laboratory angles equal to 12° and 27°, the quality of fit and the cleanness in the valley suggested that the differential cross section of the middle level at 40 MeV beam energy is less than 0.02 mb/sr in this angle range. Hence the

differential cross sections for the 6.909 and 6.948 states are believed to be fairly accurate, and the spin assignments for these two states can be made more or less unambiguiously. At larger angles good fits were still achieved, although the middle level started to show up. The angular distributions for the 6.909 and 6.948 states are shown in Figs. 11 and 16 respectively.

Calibration of Excitation Energies

The excitation energies of the observed levels of ^{40}Ca have been measured in previous works (see Section V). Below 9 MeV, every state seen in this experiment was also reported by Grace and Poletti. However, it was decided to carry out the energy calibration to check the linearity of the data accumulation system used in this work and to determine the excitation energies of those states which lie above 9 MeV.

The calibration energies for reference peaks were 3.7368 MeV (3^-), 4.4917 MeV (5^-) and 6.2850 MeV (3^-) taken from Ref. 26 and the 7.1133 state from Ref. 27. The results of the calculation are listed in Table IV. The energy shown for a given peak was obtained by averaging over the results from most of the spectra at each beam energy and again over all four energies. As can be seen in the table, the consistency of the

experimentally determined excitation energy for every state was within $\pm$10 keV. Comparisons with other experiments are discussed in Section V. No attempt was made to calibrate the energies for closely spaced multiplets.

III. DWBA AND COLLECTIVE MODEL ANALYSIS

The theory and use of the distorted wave born approximation (DWBA) and the collective model to analyze inelastic proton scattering have been presented extensively elsewhere.[28-30] In particular, we will use the procedures and terminology set forth in Reference 30.

Elastic Scattering

In order to obtain parameters for the distorted waves used in the DWBA calculations, the angular distributions of elastic scattering were analyzed for each energy using a standard optical potential (c.f. Ref. 31).

The geometrical parameters (r_o and a) for the various terms in the optical potential and the average spin-orbit strength (V_{SO}) were taken from the analysis of elastic scattering and polarization measurements for 40-MeV protons on eleven nuclei from ^{12}C to ^{208}Pb.[31] The remaining parameters, V_0, W_0, and W_D, were varied to give the best fit to the data.

The results are listed in Table V. These parameters were used for all the DWBA calculations presented in this study.

The elastic data, in ratio to Rutherford scattering, and the final optical model calculation are shown in Fig. 5.

DWBA Calculations

The DW calculations were made using a FORTRAN-IV version of the Oak Ridge computer code JULIE[32] implemented to run on the MSU Cyclotron Laboratory's XDS Sigma-7 computer. The input consists of three major parts corresponding to the elements in the integral of the transition amplitude, i.e. the form factor, the entrance channel wave function (incoming DW) and the exit channel (outgoing DW). The form factors used for the collective model deformed both the real and imaginary parts of the optical potential. Coulomb excitation was included for L-transfers of 2 and 3 in the collective model analysis. Spin-flip contributions were not included.

The entrance channel was described by the optical model parameters listed in Table V. The optical parameters for the exit channel depend on whether the Q-value was considered or not. Figure 10 summarizes the general results of the calculations for L=2 to L=8 and for energy dependence as well as the Q-value effect. For L=8, a spin-orbit term in the optical potential can not be included unless j=L (Table I, Ref. 32). In order to

estimate the effect of the spin-orbit potential on the distribution, calculations were made with and without this term in both entrance and exit channels for the case of L=6. It was found that the effect is small except for 25 MeV as illustrated.

The deformation parameters, β_L, were obtained by calculating the ratio of the cross sections σ(exp) and σ_L(JULIE), each integrated over the angular range of this experiment. The deformation, δ_L, is defined as $B_L R_o$ where R_o is the real radius of the target nucleus. R_o=3.96 F was used for all the calculations.

The experimental angular distributions of the states at 3.903 MeV (2^+), 3.736 MeV (3^-), 6.285 MeV (3^-), 6.505 MeV (4^+), and 4.491 MeV (5^-) were used as empirical standards to assist in the determination of the L-transfers to other states. It was found that most of the angular distributions with the same L at the same bombarding energy resemble each other in shape. Distributions revealing possible differences in microscopic structure and reaction mechanism were also noted. Since there are four distributions from four bombarding energies for each state which could be compared with the standards, the ambiguities in determining the L-transfer for a given state were minimized.

The L assignments to the components of a doublet were obtained from a decomposition method (see Section II). The high spin states having L=6 or L=7 were identified by fitting the data to the DWBA angular distributions.

Distorted wave collective model calculations were done for every state with appropriate adjustments for the Q-value in exit channels. Nuclear deformations were then extracted. The assigned L-values and the deformation parameters along with other physical quantities are listed in Tables VI to IX. The experimental data, the collective model fits, and the standard distributions are shown in Fig. 11 to Fig. 15 where the solid curves are collective model calculations and dashed curves show the shapes of the standard distributions.

The main features of the data presented in Fig. 11 to 15 are as follows:

1) The structure of the angular distributions becomes more pronounced as the beam energy increases, thus enabling an L-transfer assignment to be most easily achieved at the higher energy.
2) The fractional deformation parameter, δ_L, is seen to be independent of energy (over this limited energy range and within the experimental uncertainties of the data).

Figure 16 shows the experimental cross sections obtained for three L=1 states at 5.092, 6.948, and 8.274 MeV. The solid curves drawn against the data of 5.902 MeV are the results of collective model calculations. It is seen that the fits are very poor, therefore deformation parameters were not obtained

for L=1 states. A possible explanation of this result is that under the incompressibility constraint, the L=1 vibration corresponds to the oscillation of the center-of-mass of the nucleus, which, of course, is not the excitation observed. A microscopic description which accounts for the 1st and 2nd 1^- states is given in a later section of this paper.

The collective model using only the radial vibration also failed to reproduce the shapes of the distributions for the 0^+ first excited state (3.350 MeV). Calculations for this state based on a generalized collective vibrational model have been carried out by Satchler[33,29] at 25 MeV but no data were available at the time those calculations were made. In this generalized model, the potential U(V,R,a,r,) can be deformed with respect to any or all of its parameters with the constraint that the volume integral remain constant. This leads to an interaction of the form

$$\delta U = \delta R(\frac{\partial U}{\partial R}) + \delta V(\frac{\partial U}{\partial V}) + \delta a(\frac{\partial U}{\partial a})$$

DWBA calculations were made at all four bombarding energies using each of these terms and various combinations of them. Some of these calculations at 25 MeV are shown in Fig. 17. The breathing mode is the usual radial vibration ($\delta a=\delta V=0$) and the "a-vibration" calculations allow for δV and δR to be zero. The normalization of the curves to the data will

allow the normalization, β_o^2, to be determined. It is seen that the curves bear very little resemblance to the data. Similar disagreement exists at 30, 35, and 40 MeV. We also made calculations in which the parameters, V, R, and a were varied on a grid-like basis and calculations which used complex interactions within the framework of this theory. No fit was found.

We next assumed the empirical form factor of the form:

$$F(r) = \exp\left[\frac{-(r-R+a)^2}{a}\right] - B \exp\left[\frac{-(r-R+a)^2}{a}\right].$$

The choice of this form factor was made such that a node would appear in the nuclear surface region. After searching on R, a, and B, it was found that the data could be fit qualitatively using the form factor shown in Fig. 19. A comparison between the data and the calculated cross-sections using this form factor is also shown in Fig. 18. The main difference between this form factor and that of the a-vibration form factor is in the relative size of the oscillation at the surface. However, if one postulates that the ground state and the excited 0^+ state are mixed spherical and deformed, as has been suggested,[34,35] then one may expect a form factor similar to the empirical form factor.[29]

This and other microscopic considerations for this state will be discussed in Section V.

The values of δ_L for $^{40}Ca(p,p')$ are listed in Table VI for the bombarding energies 24.93 MeV, 30.04 MeV, 34.78 MeV and 39.83 MeV along with the L-transfer assignment. These values of δ_L were used with Eq. (4) of reference 30 to find the reduced transition probabilities for the ground-to-excited-state transitions. In the approximation that the excitations are described in terms of harmonic vibrations, Eqs. (2) and (3) of reference 30 were used to calculate the "force constant", C_L, and "mass transport" parameters, B_L. The results of these calculations, along with a comparison of the reduced transition probability in single-particle-units, G_{sp}, is given in Table VII. In Table VIII we list the fraction of the sum rules [Eqs. (5) and (6) of reference 30] exhausted for each transition.

IV. MICROSCOPIC DESCRIPTION

A great deal of work, both theoretical and experimental, has been directed towards the understanding of the energy level scheme and transition rates in ^{40}Ca in terms of the shell-model and its extensions.[1-6] The properties of the negative parity states in ^{40}Ca have been most vigorously investigated. The RPA seems to give a reasonably good description of the salient features of these states which are formed predominately, although not entirely, from single-particle single-hole excitations.

Positive-parity states are likely to contain large admixtures of many-particle many-hole excitations, i.e. deformed components, and are not so easily described.

Recently progress has been made in describing the (p,p') reaction in terms of a direct interaction between the projectile and target nucleons through an effective force. The properties of the effective force are largely dictated by the empirical two-nucleon potential. In particular, it has been shown by comparison with (p,p') data that the bound state reaction matrix ("bare" effective force between bound nucleons) is a good guess at the "bare" effective force in the inelastic scattering process when the laboratory energy of the projectile is in the range from 15-70 MeV.[36-38] This conclusion is based on the studies of strong, normal parity inelastic transitions and the real well of the optical potential which mainly test the strong central, iso-scalar component of the force. In these studies it was found that exchange effects are important, as was originally pointed out by Amos, Madsen, and collaborators.[36]

In the present work, microscopic DWBA calculations are performed for some of the negative parity states of ^{40}Ca and comparisons made with our (p,p') data. Random-phase-approximation state vectors of T.T.S. Kuo[39] are used for the states of ^{40}Ca in the calculation and exchange effects are included approximately[38,40] in the DWBA calculations. For further discussion on this approximation see Love and Satchler, Ref. 41.

In the following discussion, these calculations will be referred to as anti-symmetrized distorted wave (ADW) calculations. The Kallio-Kolltveit (K-K) force and the central part of the Hamada-Johnston (H-J) force are used for the projectile-target interaction. The latter is basically the same force which has been used in the RPA calculation.

Wave Functions

Extensive calculations for the ground state and the odd parity states of ^{40}Ca in terms of particle-hole configurations using the RPA method have been carried out by Gillet and Sanderson,[1,2] Kuo,[3] Leenhouts,[5] Dieperink et al.[6] and Perez.[43] Effects of spherical and deformed state mixing between the odd parity states have also been reported by Gerace and Green.[4] In addition a simple shell-model picture for this nucleus was given by Erskine,[44] Seth et al.[11] and Fuchs et al.[12]

The prediction of Gillet and Sanderson results from diagonalization of the matrix elements of the effective two-body force taken between the single-particle single-hole shell-model states. The unperturbed energy of a particle-hole configuration is the appropriate value determined by experiments. The energies for proton particle-hole states are taken from those of ^{41}Sc and ^{39}K with $\Delta E(d_{3/2}^{-1} f_{7/2})$ equal to 6.71 MeV, and for neutron states the energies are from ^{41}Ca and ^{39}Ca with

$\Delta E'(d_{3/2}^{-1}f_{7/2})$=7.37 MeV. The difference in ΔE and $\Delta E'$ is accounted for by the average Coulomb energy shift. The effective force parameter of the spin and isospin dependent Gaussian potential (central force) is 40→45 MeV and the oscillator parameter is 0.53. Isospin was not considered a good quantum number, thus their results showed strong T mixing. States with calculated level energies below 10 MeV are shown in Fig. 17 along with the results of other investigations. However, Seth et al.[11] and Fuchs et al.[12] found from proton stripping experiments that the odd parity excited states of ^{40}Ca can be explained rather well by a simple shell-model and that T-mixing of low-lying states was much less than predicted. A summary of "configuration, spin, and isospin" assignments to the ^{40}Ca negative parity states in terms of $[d_{3/2}^{-1}f_{7/2}]$ and $[d_{3/2}^{-1}P_{3/2}]$ shell-model states has been given by Fuchs et al.

In a pure RPA treatment of the odd parity spectrum of ^{40}Ca, Kuo used a G-matrix derived from the H-J potential for diagonalization. His spectrum is shown in the second column of Fig. 19 for the comparison with Gillet and Sanderson's results. Both RPA calculations encountered the difficulty of putting too much strength into the octupole transition to the ground state from the first 3^- state.

Dieperink's calculations used the modified surface delta interaction (MSDI) in both the RPA and TDA formulations, using

a $[d_{3/2}^{-1} f_{7/2}]$ splitting of 7.3 MeV. This diagonalized wave functions are very close to those of the unperturbed particle-hole states. The positions of the first four T=1 states were successfully predicted.

Gerace and Green[35] have constructed a model of mixing shell-model 1p-1h states mixed with 3p-3h deformed states to describe the odd parity states of ^{40}Ca. Their procedure was to start with RPA wave functions which were obtained using $\Delta E(d_{3/2}^{-1} f_{7/2})$=5.4 MeV. Kuo's particle-hole matrix elements were used and the effects of core polarization were included. The 3p-3h deformed states were constructed by first coupling two Nilsson orbits to obtain a 1p-1h, K=1 wave function, then recoupling this to a 2p-2h wave function to get the 3p-3h wave function. Finally matrix elements of the H-J potential between the $\langle 1p\text{-}1h|_J$ and $|3p\text{-}3h\rangle_J$ deformed states were obtained and the diagonalization was carried out. The diagonalized wave functions contain RPA wave functions and deformed $|3p\text{-}3h\rangle$ wave functions as illustrated in their paper. Their calculated spectrum is in good agreement with experimental levels below 8 MeV.

Fuchs et al. have derived the spectroscopic factors for their (d,n) work using Gerace and Green's wave functions and assuming the ^{39}K ground state to be a pure $d_{3/2}$ hole. They found that this theory agreed with experiment very well except

for a few discrepancies. Goode[44] has calculated several E2 decays for the low-lying T=0 odd parity states of ^{40}Ca, and shown that a pure RPA description of these decays is not satisfactory, whereas Gerace and Green's picture provides a consistent explanation of the B(E2) values. In comparison with the results of Goode's paper, several predictions of Gerace and Green were supported. For example, the deformed nature of the first 1^- state at 5.902 MeV and the predicted existence of the level sequence 3^-, 2^-, 4^- around 7 MeV are partially confirmed.

The purpose of this section is to summarize some of the current theoretical descriptions for the wave functions of the odd parity states of ^{40}Ca, so that one can estimate the uncertainties in the DWBA calculations due to the wave functions used. In the present paper T.T.S. Kuo's wave functions were used. However, it now appears that Gerace and Green's wave function may be more accurate.

V. RESULTS AND DISCUSSIONS OF THE MICROSCOPIC DESCRIPTION

Calculations were performed for the 1st 1^-, T=0 state; 1st 2^-, T=0 and T=1 states; 1st, 2nd, and 3rd 3^-, T=0 states; 1st 3^-, T=1 state; 1st 4^-, T=0 and T=1 states; 1st 5^-, T=0

and T=1 states; and 6^-, T=0 and T=1 states. The 1st 3^-, T=0; and 1st 5^-, T=0 states have also been investigated by Schaeffer and Petrovich.[37,38] Comparison with the results of these authors and discussion on the calculations in this paper will be presented in the following subsections.

The 1^-, T=0 State (6.948 MeV)

The major p-h components of the wave functions for the first RPA 1st 1^- state are $[2p_{3/2}d_{5/2}^{-1}]$, $[2p_{3/2}d_{3/2}^{-1}]$ and $[f_{5/2}d_{5/2}^{-1}]$. The calculated angular distributions at 40 and 25 MeV are best fit by the distributions of the 2nd experimental 1^- (6.948 MeV) state. Figure 20 shows good agreement both in shape and magnitude between theory and experiment if so assigned. Gerace and Green's calculations show that the 1st 1^- state is strongly deformed whereas the 2nd 1^- is a very pure 1^- shell-model state. Thus the assignment of the RPA 1st 1^- state to the 2nd experimental 1^- state is supported by Gerace and Green's theory.

The 1st 3^-, T=0 State (3.736 MeV)

The ADW calculations for the lowest 3^- state (3.736 MeV) have been previously reported by Petrovich and McManus,[38] and Schaeffer.[37] The results of our calculations are shown in Fig. 21. For this 3^- state the magnitudes and positions of the

maxima are well reproduced at each beam energy. The overall shapes of the experimental distributions are also in qualitative agreement, which indicates that the energy dependence of the exchange effects has been correctly accounted for. It can be seen from Fig. 21 that the contributions from exchange become increasingly important at lower energies.

Calculations which use a 1F. range "KK equivalent" Yukawa force with an empirical strength normalization are also illustrated in Fig. 21. The distributions are very similar to those obtained by using the KK+EX force. The results of a central Hamada-Johnston force plus exchange are not shown because the shapes of the calculated distributions (in direct, exchange and total) were found identical to those using KK+EX forces, except that the predicted magnitudes were found to be about 25% lower. This similarity also applies to the calculations for the 2nd 3^- (6.285 MeV) and the 5^- (4.491 MeV) states.

Schaeffer[37] has performed similar calculations for ^{40}Ca with proton energies from 17.3 to 55 MeV. He used the Blatt-Jackson potential and Gillet and Sanderson's wave functions. The dependence of exchange effects upon the energy was investigated by examining the ratio of the total cross section $\sigma[D+E]$ to the direct cross section $\sigma[D]$. A comparison of the results of his calculations with those obtained in this work are given in Table IX.

The 2nd and 3rd 3^-, T=0 States (6.285 and 6.581 MeV)

Figure 22 shows the results of the calculations for the 6.285 MeV state using direct, exchange, and a direct plus exchange force. The experimental cross-sections are again well reproduced except at 40 MeV and at large angles where the exchange contributions are overestimated.

A comparison of the experimental angular distributions between this 3^- and the 1st 3^- state reveals some differences which may be attributed to the nuclear wave functions or to the mechanism of the interaction or both. The agreement between the ADW calculations and the experimental results seems to suggest that the RPA descriptions for this state are quite good. However, difficulties were encountered when the ADW calculations for the 3rd RPA 3^- state were compared with the distributions of the 3rd 3^- of the experimental spectrum. It was found that the calculated cross sections were 10 times too low, as can be seen in Fig. 25. On the other hand, This discrepancy was resolved in the extended shell-model calculations of Gerace and Green[4] their 3rd 3^- state is essentially the 2nd RPA 3^- state and their 2nd 3^- is a mixture of the 3p-3h deformed state as well as contributions from the 1st and the 2nd RPA 3^- states. The electric transition rates to the ground state from the 2nd and 3rd 3^- states Gerace and

Green are about equal (1.9 vis 2.7 single-particle units), thus their picture is consistent with the excitation strength measured in this experiment (2.5 vis 1.7 single-particle units).

The 5^-, T=0, 1 States (4.491 and 8.535 MeV)

The ADW calculations using T.T.S. Kuo's wave functions for the 5^-, T=0 (4.491 MeV) state are shown in Fig. 23. The exchange term dominates the contribution to give the correct magnitude of the differential cross sections but overshoots somewhat at large angles. The contributions from the direct term are small as can be seen from Fig. 23 and the $\sigma[D+E]/\sigma[D]$ ratio in Table IX. The ADW calculations for this state demonstrate the extreme importance of the exchange effect in predicting the correct magnitude of the angular distributions.

The calculated distribution of the 1st 5^-, T=1 state using T.T.S. Kuo's wave functions are shown in Fig. 25. The distributions of the components LSJ=505 and 515 were found comparable in magnitude. The total distribution is the incoherent sum of these two components. The corresponding experimental results show that the calculations predict the correct normalization.

The particle-hole configurations of these RPA 5^-, T=0 and 1 states are mainly $[f_{7/2}d_{3/2}^{-1}]$, in good agreement with the results of (^{3}He,d) and (d,n) measurements (12,13,14) and with the theory of Gerace and Green.[4]

The Unnatural Parity States

The ADW calculations were done using T.T.S. Kuo's wave functions for the 2^-, T=0 state (6.026 MeV) at four energies, and for the 2^-, T=1 state (8.418 MeV) at 25 and 40 MeV. The results are illustrated in Fig. 24. At E_p=40 MeV, both T=0 and T=1 states are qualitatively reproduced. At the lower energies the calculations systematically underestimate the differential cross sections at small angles. Because of the similarity both in shape and cross section, this experiment could not distinguish between the RPA and deformed 2^-, T=0 states. This leaves an ambiguity in this experiment in the interpretation of the states at 6.026 and 6.751 MeV.

The results for the first 4^-, T=0 and T=1 states are shown in Fig. 25. The predicted differential cross section for the 4^-, T=0 state is about 20 times lower than the experimental results of the 5.617 MeV state (see Fig. 14). On the other hand, this theoretical distribution resembles in shape the experimental counterpart. For the 4^-, T=1 state, the predicted magnitude of the cross section is about 1/2 of the estimated experimental results (the 4^-, T=1 level at 7.656 MeV was not resolved, but a few clean spectra enabled the estimation of the cross section to be made). It is also noted that both calculated distributions of the 4^-, T=0 and T=1 are similar.

Results for the 6^-, T=0 and T=1 states were also obtained as shown in Fig. 25. The experimentally observed level at 8.850 MeV (L_p=7) may be assigned to the theoretical 6^-, T=1 state. The assignment of the 9.237 MeV L=7 level to the theoretical 6^-, T=0 state is also plausible, because the predicted differential cross sections are for this state close to those of the 9.237 MeV level. Both of these states are predicted to have excitation energies between 12 and 13 MeV in the microscopic calculations. However, the experimental excitation energies are approximately consistent with them being the 6^- states of a rotational band starting at the 5.902 MeV 1^- state.

The RPA wave functions of the unnatural parity states used above can all be qualatively described as pure single particle-hole states. They are

RPA 1st 2^-,	T=0	$f_{7/2}d_{3/2}^{-1}$
RPA 1st 2^-,	T=1	$2p_{3/2}2s_{1/2}^{-1}$
RPA 1st 4^-,	T=0,1	$f_{7/2}d_{3/2}^{-1}$
RPA 6^-,	T=0,1	$f_{7/2}d_{5/2}^{-1}$

The similarities in the wave functions of the 4^- and 6^- states, as well as the differences between the 2^-, T=1 states are also reflected by the calculated distributions, as expected. Gerace and Green's deformed model agrees with the RPA description

of the lst 4^- state. This $[f_{7/2}d_{3/2}^{-1}]$ configuration has been confirmed by Erskine,[43] Seth et al.,[11] and Fuchs et al.[12] in their [^{3}He,d] and [d,n] experiments respectively. Thus the wave functions of this state are believed to be well understood. The failure of ADW calculation for this particular state must be due to the effective force used. Perhaps the tensor force or spin-orbit force will play an important role in regaining the correct normalization. For example, it was found by Love[43] in calculating ^{90}Zr(p,p') cross-sections that the highest spin transfer was dominated by the two-body spin-orbit interaction. The spin-orbit force is also important[45] in the excitation of the unnatural parity z-state at 8.87 MeV in ^{16}O.

The Even-Parity States

Figure 26 shows all of the even-parity states observed in this experiment. The spacing between the vertical lines is in accord with a J(J+1) relationship. The length of the horizontal lines is proportional to the transition strength. The open circles are for those states observed in other experiments (see Table X).

The low-lying even-parity states of ^{40}Ca have been described in terms of multiparticle-multihole configurations by Gerace and Green[35,40] and by Federman and Pittel.[48,49]

In the paper[35] of Gerace and Green some of the low-lying states are considered as mixtures of the double closed 2s-1d shell-model state (j=0) with two intrinsic deformed states (containing components with even angular momenta) formed by raising 2 and 4 particles from the $1d_{3/2}$ shell into the 2p-1f shell. Their results are shown in Table XI. The first calculated sequence appears to correspond to the experimentally observed 3.350(0^+), 3903(2^+) and 5.279(4^+) states, which seem to form a nearly perfect rotational band (see Fig. 26). In the second calculated sequence, the 8.00 MeV level may be either the observed 7.923 or 8.100 MeV level. This 2p-2h sequence does not follow the J(J+1) relationship and no discussion of this aspect was given. Gerace and Green[48] also used their deformed model and mixing technique to account for the 5.212 MeV (0^+) and 5.249 MeV (2^+) states. K-band mixing and 6p-6h, 8p-8h deformed rotational bands were included. Their previous calculations were modified to allow complete mixing between 0p-0h, 2p-2h, 4p-4h, 6p-6h, and 8p-8h configurations. Anderson et al.[51] compared their (p,p'γ) results with Gerace and Green's picture. A K=2, 4p-4h band for 5.249(2^+), 6.026(3^+) and 6.505(4^+) MeV levels, and a K=0 8p-8h band for 5.249(0^+), 5.627(2^+) and 6.544(4^+) MeV levels were constructed based on the enhancement of the in-band transitions. The former band does not obey the J(J+1) law whereas the later does (see Fig. 26).

Anderson et al. found that there was a general agreement between the experimental reduced matrix elements and the theoretical values for the 4p-4h and 8p-8h states.

Federman and Pittel[47] have shown that an alternative description for the low-lying 0^+ levels of ^{40}Ca is possible which does not require a 6p-6h or 8p-8h state. They proposed a weak coupling model in which the energies of the known 0^+ states are 3.29, 5.22, 7.62 MeV, in excellent agreement with the experimental 0^+ states at 3.350, 5.212, and 7.300 MeV. The same model was also applied to the 2^+ states[50] and all eight 2^+ states were well reproduced by the calculated spectrum. It should be noted that Gerace and Green's model attempted to retain the band structure of the deformed even-parity states, whereas Federman and Pittel's model emphasized only the configurations of the spectrum of a given even J; thus no calculation was made for 4^+ states. These two models have enjoyed success in different areas and a comparison between them can only be made by an experiment on electromagnetic transitions between those states covered by both areas of studies.

So far, all the observed 0^+ and 2^+ states and those 4^+ states below 7 MeV have been theoretically investigated. However, the 4^+ states above 7 MeV and the 6^+ states in this experiment may bring new information out of the band structures

of the even-parity states in ^{40}Ca. Further theoretical and experimental studies on this aspect are desired.

The 1st Excited 0^+ State (3.350 MeV)

There is a general agreement between the Gerace and Green (GG)'s and the Federman and Pittel (FP) models that the 3.35 MeV level in ^{40}Ca is mainly a 4p-4h deformed state. The 4p-4h strength predicted is about 70% by GG model and is about 83% by FP model. The $^{42}Ca(p,t)^{40}Ca$ experiment[50] showed that if the ground state of ^{40}Ca is assumed to be a pure 0p-0h (shell-model) state, the 3.350 MeV 0^+ state is certainly not a pure 2p-2h state. This evidence complements the GG and FP results.

The configuration of the ground state of ^{40}Ca is described mainly by 0p-0h (82%) mixed with 2p-2h (17%). This mixture has been supported by $^{40}Ca(p,d)$ $^{40}Ca(^3He,^4He)$ reactions[51] and also by the $^{39}K(^3He,d)$ experiment.[11] If one compares the wave functions of the ground state and those of the 1st excited 0^+ state predicted by the GG model, such as

Ground state:	0p-0h(0.91);	2p-2h(0.41)
3.35 MeV state:	4p-4h(-0.83)	6p-6h(-0.45)

one finds that the 3.35 MeV state might be predominately a 4p-4h excitation from the ground state as a whole.

In section III, it was mentioned that the (p,p') data obtained in this experiment could only be fit using an empirical form factor shown in Fig. 18, and that the fit is very sensitive to the relative size of the oscillation in the surface. If a form factor, calculated by using 4p-4h wave functions and appropriate effective interaction, could be obtained, it would be interesting to see the comparison between this theoretical form factor with the empirical one.

An alternate possibility for explaining the observations on the 0^+ may lie in a two-step process such as picking up two neutrons in the spherical ground state and returning them to the deformed excited 0^+ state. At 40 MeV the reaction $^{40}Ca(p,t)^{38}Ca(g.s.\ 0^+)$ has a similar angular distribution.[52] The main difference is that the (p,t) angular distribution has a deeper valley than does the inelastic scattering presented here.

VI. COMPARISONS WITH OTHER EXPERIMENTS

Energy Levels

Figure 27 presents the levels seen in this (p,p') experiment along with representative spectra from other types of reactions. The energies of the low-lying levels have been determined with high prescision by high resolution (p,p')[52,25] and γ-ray measurements.[53,26] The energies given in this work were obtained by a calibration which used Grace and Poletti's results.

As can be seen from Fig. 27, there is good agreement between the results of the present experiment and that of Grace and Poletti from 3.350 MeV to 8.850 MeV excitation energy. The 5.212 MeV and 6.544 MeV states were too weakly excited to be seen in this experiment. Above 7 MeV, the (α,α') experiment recorded only a few levels due to experimental limitations.

Spin Identification

The J^{π} assignments of the excited states of ^{40}Ca obtained from various experimental sources are summarized in Table X. Some of this information has been reported by Seth et al.[11] Since then many new results on spin assignments for the excited levels of ^{40}Ca, including those from this experiment, have become available.

States Below 6.58 MeV

The spins and parities of low-lying levels below 6.58 MeV have been well determined. The most complete set of spin assignments was given by Anderson et al.[49] who have done extremely precise $(p,p'\gamma)$ measurements. A summary of the previous assignments has been discussed by Seth et al.[11] The spins and parities of $3.350(0^+)$, $3.736(3^-)$, $3.903(2^+)$, $4.491(5^-)$, $5.617(4^-)$, $5.902(1^-)$, $6.026(2^-)$, $6.285(3^-)$, and $6.581(3^-)$ MeV excited states are consensus assignments. Of the triplet at

5.212-5.249-5.279 MeV the 5.212 state, which was not seen in this experiment, has been dentified as 0^+ by all of the most recent $(p,p'\gamma)$ studies.[26,50,55]

Individual angular distributions for the 5.249 and 5.279 MeV states were obtained (see Fig. 11 and Fig. 13) and are assigned L=2 and L=4. The assignments are in agreement with results of (p,γ) and $(p,p'\gamma)$ experiments.[56,5,57]

The 5.627 MeV component of the 5.617 MeV doublet has been identified as 2^+ by many γ-decay experiments. In this work, the angular distributions of this doublet permit a small mixture of L=2 strength to the dominant L=5 strength. The upper limit of the L=2 contributions was determined to be ($\delta_2 \lesssim 0.09$). The value of B(E2) in Weisskop units, i.e., G(sp), based on this estimated deformation is in qualitative agreement with other electromagnetic transition measurements. On the other hand, the (α,α') experiment by Lippincott et al.[7] observed only the 2^+ component, indicating that this state is observed in both types of inelastic scattering.

The 6.029 MeV level of the 6.025-6.029 MeV doublet was discovered by Grace and Poletti. It is assigned as having $J = 3^+$, but 2^- was not entirely ruled out according to Anderson et al. In the present experiment, this doublet was observed to be an L=3 transfer as a whole.

Anderson et al. are the only group who identify the 6.544 MeV level as 4^+. In the present experiment the 6.505 MeV level was well resolved from the 6.581 MeV state (see Fig. 2) and found to be a 4^+ state. However, the 6.544 MeV level was not seen at all. It may be the case that this state was weakly excited with respect to the 6.505 MeV level and because it is also a 4^+, the analyzed group may actually be a 4^+-4^+ doublet.

States Between 6.750 and 7.558 MeV Excitation Energy

The 6.751 MeV level: This state has been assigned as $(2,0)^-$. Seth et al.,[11] working in the $^{39}K(^3He,d)$ reaction prefer 0^-. However, Fuchs et al., who have done the $^{39}K(d,n)$ experiment[12] to unfold the problem of the missing 2^- strength of the T=0 quartets of the $[d_{3/2}^{-1}f_{7/2}]$ and $[d_{3/2}^{-1}p_{3/2}]$ configurations, contend that this 6.751 MeV state should be assigned as 2^- based on an observed L=3 transition, as opposite to the L_p=1 assignment obtained by Seth et al. They interpret this state as the 2^- component of the $[d_{3/2}^{-1}f_{7/2}]$ quartet. In the present (p,p') experiment, the 6.751 MeV level was observed to be excited by an L=3 transfer indicating that the (p,p') reaction favors the 2^- assignment or possibly 3^- (see Fig. 12). Resolution of the discrepancy between the contradictory results of the (d,n) and (^{3}He,d) reactions can be found partly from Gerace and Green's calculations[4] based on the mixing of $\overline{3p\text{-}3h}$ deformed states with the shell-model states of T.T.S. Kuo.[3]

The wave function of the second 2^- state from Gerace and Green's calculations shows that it contains about 29% of $|\overline{3p\text{-}3h}>$, and 69% of $\psi_1^{2^-}$ (KUO), in which $[d_{3/2}^{-1}f_{7/2}]$ is the largest component.[3] Hence the theoretical configurations proposed for the second 2^- state are [deformed] plus the $[d_{3/2}^{-1}f_{7/2}]$. The predicted energies for the first and second 2^- states are 6.4 and 6.185 MeV which closely agree with the experimental values of 6.026 and 6.751 MeV if the latter is assigned to 2^-. The agreement between theory, (d,n), and this (p,p') experiment suggests that the 2^- assignment is favored for the 6.751 MeV state.

The 6.909-6.930-6.948 MeV triplet: Individual angular distributions for the 6.909 and 6.948 MeV states were obtained and their L-transfers are positively assigned as 2 and 1 (see Fig. 11 and Fig. 16). Metzger,[57] using γ-resonance absorption techniques has concentrated his effort on this triplet, and he identified the first and third members as 2^+ and 1^-. The 6.948 MeV level has also been assigned 1^- by proton stripping reactions. As has been mentioned in Section II, where the analysis of this triplet was discussed in detail, the middle level of 6.930 MeV may be a high spin state (≥ 3).

The 7.114 level: The spin and parity of this state has been tentatively assigned $(3)^-$ by many authors. This assignment was first given by Gray et al. in a (p,p') experiment. This

level was also observed by the (α,α') reaction[7] although no spin identification was made. An L=1 transition observed for this state in $(^3He,d)$[44,11,59] and (d,n)[12] reactions leads to the $(3)^-$ assignments by these authors.

A contradictory result was found in the present (p,p') experiment. The angular distributions of this state resemble those having L=5 transfer and are very similar to those of the 5.617 MeV state (see Fig. 14). At E_p=25 MeV, the distributions of these two levels agree very well with the L=5 collective model predicition. At E_p=40 MeV, the distribution are intermediate between L=5 and L=4. In any case, the angular distributions of the 5.617 and 7.114 MeV states are remote from those of L=3 transfer. Other evidences of similarity between these two levels can be seen from the $^{39}K(p,\gamma)$ experiment performed by Lindeman et al.[57] The gamma-ray branchings of both the 5.617 and 7.114 MeV levels were found to be about the same, namely 70% to the 3.74 MeV level and 30% to the 4.49 level.

The forementioned calculations by Gerace and Green suggest that the second 4^- state is essentially a collective state with over 80% of $\overline{3p\text{-}1h}$ strength. The predicted energy is 7.65 MeV. Thus, it is possible that the 7.114 MeV level corresponds to the second 4^- of Gerace and Green's scheme. The L=1 stripping transition to this state cannot, perhaps, be interpreted by the simple particle-hole picture of the shell-model. The present

data on the 7.114 MeV state are most consistent with a 4^- assignment but the disagreement with the proton stripping remains unresolved.

The 7.543 MeV Doublet: The 7.531 MeV state has been observed in (^{3}He,d) and (d,n) experiments and tentatively assigned as $(2)^-$, based on the shell-model. In the present experiment, this and the 7.558 MeV levels are not separated and were analyzed by decomposition (Section II). The 7.531 MeV level is found to be excited by an L=3 transfer in agreement with the results of proton stripping reactions. The 7.558 MeV state is identified as an L=4 transfer. The 7.57 MeV level observed in the (α,α') experiment[7] may correspond to this state.

T=1 Analog States

The T=1 analog states of ^{40}K have been assigned by Erskine at 7.655(4^-), 7.696(3^-), 8.414(2^-), and 8.535(5^-) MeV. His proposal was based on the results of his (^{3}He,d) data and on Enge's (d,p) experiments[43,60] and of the observation of the lowest T=1 state in ^{40}Ca by Rickey et al.[61] The energy of this state has also been measured by Kashy and Snelgrove.[62] These experimental results also agree with the calculated excitation for the lowest ^{40}K analog states in ^{40}Ca in the

$[d_{3/2}^{-1}f_{7/2}]$ configuration. Experimentally, this has been further investigated by Seth et al. and Fuchs et al. Both groups have confirmed Erskine's identification. Fuchs et al. even extended this technique to identify the T=1, $[d_{3/2}^{-1}p_{3/2}]$ quartet.

In the present experiment, the 7.655, 7.676, 7.696 MeV triplet was not resolved and the J^{π}-values of the 7.655 and 7.696 MeV states are taken from the results of authors mentioned above. The 8.418 and 8.535 MeV levels are observed to be L=3 and 5 transitions respectively, consistent with the 2^- and 5^- results of the stripping reaction experiments. The $[d_{3/2}^{-1}p_{3/2}]$ T=1 quartet was proposed by Fuchs et al. to consist of the 10.051(0^-), 9.435(1^-), 9.408(2^-), and 9.404(3^-) MeV levels. At Ep=35 MeV, a level at 10.051 MeV is seen having L=5 transfer. No angular distribution for the 9.435 MeV state was obtained here. A doublet at 9.413 MeV with an L=3 angular distribution was observed which could possibly correspond to the 2^- and 3^- levels at 9.408 and 9.404 MeV.

States Between 7.6 and 8.8 MeV

Aside from the T=1 analog states discussed in the last section, there are a few even-parity states which lie in this region. The 7.869, 8.092, 8.578, and 8.747 MeV levels were identified as having an L=2 transfer and the 7.923, 8.366 MeV

levels as L=4, in agreement with the results of (α,α') experiments. It is interesting to observe from Table X that the (α,α') experiments excited none of the T=1 states as expected from the selection rule $\Delta T=0$ for the inelastic scattering of alpha particles.

There are two L=1 states observed in this region. The 8.274 MeV level (see Fig. 16) is tentatively assigned as a doublet with possible spins of (0^-) and (2^+). The 0^- component of the T=0 $[d_{3/2}^{-1}p_{3/2}]$ quartet was tentatively assigned by Fuchs et al. to be one of the 8.274 or 8.366 or 8.933 levels. In the present experiment the 8.933 MeV level was very weakly excited (about 30 ± 10 μb-sr at 30° and 8 ± 4 μb/sr at 60° at E_p=25 MeV) and no angular distribution could be obtained. The 8.366 MeV level has been identified as an L=4 transfer in this and two (α,α') experiments.

The 8.113 MeV level is taken to be $(1,2,3)^-$.

The High L-Transfer States and Levels Above 9 MeV

Several states having spins possibly equal to 6 or greater were observed. The characteristics associated with high L-transfer in the (p,p') reaction is that the angular distributions of such excited states peak at large scattering angles as can be seen in Fig. 15. The 8.191 and 8.978 MeV levels are observed with L=6 transfer, and their J-values are tentatively assigned as 6^+.

The angular distributions for the 8.850 MeV state show systematic agreement with an L=7 collective model prediction at four beam energies. This state is tentatively assigned $J^{\pi}=(6^{-})$ since this is the highest spin, negative parity state that can be made in any relatively simple way from the ^{40}Ca ground state. The same assignment could possibly be given to the 9.237 MeV level but with less confidence, for there is only one angular distribution analyzed and compared with theory.

Further investigations by other types of reactions are needed to confirm these findings.

Due to the very high density of states above 9 MeV exciation, detailed identification of states is hazardous.

Comparisons of β_L's and G's

Table XII compares the experimental nuclear deformations, β_L, we obtained with those from previous experiments. For six beam energies and three independent experiments, the deformation for the 3.736 MeV (3^{-}) state was found to be more or less a constant 1.4 F. The observations of two (α,α') measurements are consistent with each other and incidentally very close to the (e,e') result, but only 2/3 of those obtained from (p,p').

The deformation of the 3.903 MeV(2^{+}) state is independent of proton energy as well as the type of scattering particle.

Other even-parity states show about the same trend. For the 4.491 MeV(5^-) state, the (p,p') deformation is again about twice as large as the (α,α') findings. The results for the 6.285 MeV state are quite consistent in every case except (e,e'). The qualitative agreement between (α,α') and (p,p') experiments on the 6.577 state can also be noted, except for the 17 MeV (p,p') work.

It appears that the deformations extracted at higher energy are consistently smaller than those at lower energies in both (p,p') and (α,α') experiments. This trend of energy dependence may result from the model and analysis procedure used.

A comparison of the reduced transition probabilities with (e,e') and γ-decay experiments is made in Table XIII. Only those transitions with 100% to ground state branching, i.e., B(EL; 0→L) are compared. As can be seen from the table, the G-values obtained in this experiment agree very well with the majority of all other results, especially those of Eisenstein et al.[10] It has been pointed out by these authors that their findings are relatively parameter or model independent.

A comparison of B(pp'; 0→L) and B($\alpha\alpha'$; 0→L) is shown in Table XIV. The major discrepancies occur at high excitation eneriges where the (α,α') results are seen to be consistently high except for the 4.491 MeV state. This is believed to be in part due to the fact that alpha scattering was done with less resolving power.

The reduced transition probabilities B(EL) scaled for the (p,p') experiment were obtained using Fermi-equivalent uniform-density-distributions.

VII. SUMMARY

The angular distributions for protons inelastically scattered from various excited states of ^{40}Ca have been measured at incident proton energies of 25, 30, 35 and 40 MeV. Data for about 50 states have been analyzed and the systematic and consistent variations of the distributions with respect to the proton beam energy were observed. The L-transfer for most of the observed states have been compared with the results of other experiments. Good agreement was obtained in general and some ambiguities that existed in previous experiments were clarified. It is concluded that the (p,p') experiment, performed at relatively high proton energies with a good-resolution detection system, enables one to determine the L-value with less uncertainty. States with spin-transfer larger than 5 have been observed and identified.

The DWBA collective model analysis has been carried out and the deformations δ_L's were extracted. It was found that the collective model was successful in predicting angular distributions in agreement with this experiment, except for the

cases of L=0 and L=1, where it is known to be an incorrect description. Generally speaking, the collective DWBA distributions follow the same energy dependence patterns as those of the experimental observations. It also appears that the overall shape and magnitude of the experimental angular distributions of a given L are roughly independent of excitation energy. Therefore, the δ's extracted are more or less energy independent. However, this statement does not apply to every excited state. For example, the individual distributions of the 6.751 MeV state coincide in shape with those of the 3.736 MeV state, but the relative magnitudes in going from one energy to the next do not. Thus the observed energy dependence of δ for this 6.751 MeV state may be real and interpretations for this phenomenon are to be desired.

Finally, the antisymmetrized distorted wave calculations have been performed for some negative parity states, using the K-K force and T.T.S. Kuo's RPA wave functions. The particle-hole configurations of these states were investigated by examining the overall results of these ADW calculations and comparing them with other theoretical and experimental results. The nature of the states under study are fairly well understood. It was also found that the central force used in the ADW calculations is adequate in predicting the distributions of the normal parity states, but a non-central force may be essential to reproduce those of the unnatural parity states.

ACKNOWLEDGEMENTS

We would like to express our gratitude to all of the staff at the Michigan State University Cyclotron Laboratory for making this work possible. In particular we wish to express thanks to our colleagues, Professors S. Austin, G. Bertsch, G. Crawley, W. Kelly, and H. Wildenthal for their many invaluable discussions and comments.

REFERENCES

1. V. Gillet and E.A. Sanderson, Nucl. Phys. 54, 472(1964).
2. V. Gillet and E.A. Sanderson, Nucl. Phys. A91, 292(1967).
3. T.T.S. Kuo and G.E. Brown, Nucl. Phys. 85, 40(1966).
4. W.J. Gerace and A.M. Green, Nucl. Phys. A113, 641(1968).
5. H.P. Leenhouts, Physica 35, 290(1967).
6. A.E.L. Dieperink, H.P. Leenhouts, and P.J. Brussaard, Nucl. Phys. A116, 555(1968).
7. E.P. Lippincott and A.M. Bernstein, Phys. Rev. 163, 1170(1967); E.P. Lippincott, Thesis (1967), MIT.
8. A. Springer and B.G. Harvey, Phys. Letters 14, 116(1965).
9. D. Blum, P. Barreau, and J. Bellieard, Phys. Letters 4, 109(1963).
10. R.A. Eisenstein, D.W. Madsen, H. Theissen, L.S. Cardman, and C.K. Bockelman, Phys. Rev. 188, 1815(1967).
11. K.K. Seth, J.A. Biggerstaff, P.D. Miller, and G.R. Satchler, Phys. Rev. 164, 1450(1967).
12. H. Fuchs, K. Grabisch, and G. Roschert, Nucl. Phys. A129, 545(1969).
13. A. Tellez, R. Ballini, J. Delannay, and J.P. Fonan, Nucl. Phys. A127, 438(1969).
14. H.G. Blosser, Communication and Electronics, January 1961.
15. H.G. Blosser and A.I. Galonsky, IEEE Trans. on Nuclear Science, NS-13, No. 4, 466(1966).

16. M.M. Gordon, R.E. Berg, and H.G. Blosser, Nucl. Instr. and Methods 58, 327(1968).

17. G.H. Mackenzie, E. Kashy, M.M. Gordon, and H.G. Blosser, IEEE Trans. on Nuclear Science, NS-14, No. 3, 450(1967).

18. J.L. Snelgrove and E. Kashy, Nucl. Instr. and Methods 52, 153(1967).

19. W. Benenson, R. deForest, W.P. Johnson, E. Kashy, Nucl. Instr. and Methods 64, 40(1968).

20. K. Thompson, Ph.D. Thesis, Michigan State University (1969).

21. C.R. Gruhn, T. Kuo, C. Maggiore, B. Preedom, L. Samuelson, and J. Chander, IEEE Trans. Nucl. Science 15, No. 3, 337(1968).

22. L.H. Johnston and D.A. Swenson, Phys. Rev. 111, 212(1958).

23. J.F. Janni, Air Force Weapons Laboratory Report, AFWL-TK-65-150 (1966).

24. J.M. Cameron, TEchnical Report P-80 University of California, Los Angeles, California (1967); Phys. Rev. 167, 908(1968).

25. M.A. Grace and A. R. Poletti, Nucl. Phys. 78, 273(1966).

26. A.R. Poletti, A.D.W. Jones, J.A. Becker, and R.E. McDonald, Phys. Rev. 181, 1606(1969).

27. K.W. Dolan and D.K. McDaniels, Phys. Rev. 175, 1446(1968).

28. G.R. Satchler, Nucl. Phys. 55, 1(1964).

29. G.R. Satchler, Nucl. Phys. A100, 481(1967).

30. B.M. Preedom, C.R. Gruhn, T.Y.T. Kuo, and C.J. Maggiore, Phys. Rev. C2, 166(1970).

31. M.P. Fricke, E.E. Cross, B.J. Morton, and A. Zucker, Phys. Rev. 156, 1207(1967).

32. R.H. Bassel, R.M. Drisko, and G.R. Satchler, Oak Ridge National Laboratory Report No. ORNL-3240, 1962 (unpublished); and Oak Ridge National Laboratory Memorandum to the Users of the Code JULIE, 1966 (unpublished).

33. G.R. Satchler, Private Communication with C.R. Gruhn, 1966.

34. G.E. Brown and A.M. Green, Nucl. Phys. 75, 410(1966).

35. W.J. Gerace and A.M. Green, Nucl. Phys. A93, 110(1967).

36. K.A. Amos, V.A. Madsen, and I.E. McCarthy, Nucl. Phys. A94, 103(1967).

37. R. Schaeffer, Nucl. Phys. A132, 186(1969).

38. F. Petrovich, H. McManus, V.A. Madsen, and J. Atkinson, Phys. Rev. Letter 22, 895(1969).

39. T.T.S. Kuo, Private communication with H. McManus (1966).

40. F. Petrovich, Ph.D. Thesis, Michigan State University, (1970).

41. W.G. Love and G.R. Satchler, Nucl. Phys. A159, 1(1970).

42. S.M. Perez, Nucl. Phys. A136, 599(1969).

43. J.R. Erskine, Phys. Rev. 149, 854(1966).

44. P. Goode, Nucl. Phys. A140, 481(1970).

45. S.M. Austin, R. Schaeffer, and W. Benenson, private communication with C.R. Gruhn (1971).

46. W.J. Gerace and A.M. Green, Nucl. Phys. A123, 241(1969).

47. P. Federman and S. Pittel, Nucl. Phys. A139, 108(1969).

48. P. Federman and S. Pittel, Phys. Rev. 186, 1106(1969).

49. R. Anderson, A. G. Robertson, D.F.H. Start, L.E. Carlson, and M.A. Grace, Nucl. Phys. A131, 113(1969).

50. S.M. Smith and A.M. Bernstein, Nucl. Phys. A125, 339(1969).

51. C. Glashausser, M. Kondo, M.E. Rickey, and E. Rost, Phys. Letters 14, 113(1965).

52. R. Paddock, Ph.D. Thesis (1969).

53. A. Marinov and J.R. Erskine, Phys. Rev. 147, 826(1966).

54. K.W. Dolan and D. K. McDaniels, Phys. Rev. 175, 1446(1968).

55. J.R. MacDonald, D.F.H. Start, R. Anderson, A.G. Robertson, and M.A. Grace, Nucl. Phys. A108, 6(1968).

56. H.P. Leenhouts and P.M. Endt, Physica 32, 322(1966).

57. H. Lindeman, G.A.P. Engelbertink, M.W. Ockeleon, and H.S. Pruys, Nucl. Phys. A122, 373(1968).

58. F.R. Metzger, Phys. Rev. 165, 1245(1968).

59. J.S. Forster, K. Bearpark, J.L. Hutton, and J.F. Sharpey-Schafer, Nucl. Phys. A150, 30(1970).

60. H.A. Enge, E.J. Irvin, and D.H. Weaner, Phys. Rev. 115, 949(1959).

61. M.E. Rickey, E. Kashy, and D. Knudsen, Bull. Am. Phys. Soc. 10, 550(1965).

62. E. Kashy and J.L. Snelgrove, Phys. Rev. 172, 1124(1968).

63. L.N. Blumberg, E.E. Gross, A. van der Woude, A. Zuker and R.H. Bassel, Phys. Rev. 147(1966)812.

64. B.W. Ridley and J.F. Turner, Nucl. Phys. 58(1964)497.

65. W.S. Gray, R.A. Kenefick and J.J. Kraushaar, Nucl. Phys. 67(1965)542.

66. K. Yagi et al., Phys. Letters 10(1964)186.

67. J.R. MacDonald, D.F.H. Start, R. Anderson, A.G. Robertson and M.A. Grace, Nucl. Phys. A108(1968)6.

Table I. Isotopic Analysis of ^{40}Ca Target Used

	Isotopic Analysis (Atomic Percent)
^{40}Ca	99.973%
^{42}Ca	0.008
^{43}Ca	0.001
^{44}Ca	0.018
^{46}Ca	<0.001
^{48}Ca	0.001

Table II. Contributions to the Energy Resolution (40 MeV Protons)

Sources	ΔE(keV)
Straggling	
Target	10.0
Package Windows	5.3
Detector Windows	8.0
Total	23.3
Electronic	7.2
Ion Pair Statistics	7.3
Beam Spread	10.0
Kinematic (at 45°)	7.5
Overall	28.3

Table III. Absolute Cross-section Measurement Comparison

Target	E_p	θ_{CM}	Present Experiment $\frac{d\sigma}{d\Omega} \pm \Delta$* (mb)±(%)	$\frac{d\sigma}{d\Omega} \pm \Delta$ (mb)±(%)	Absolute Error (%)	Reference
^{12}C	40	60°	10.6±2.4	10.3±2.0	5.0	a
^{16}O	40	50°	20.2±2.0	20.2±1	1.7	b
^{40}Ca	40	41°	96.2±0.2	96.7±2.0	5.0	a
^{40}Ca	30	46°	109.6±0.2	110.1±1.7	3.0	c

*Statistical Error Only.

a) Reference 63
b) Reference 24
c) Reference 64

Table IV. Excitation Energy Measurements, ^{40}Ca

E_p=25 MeV $E^* \pm \Delta E$ (keV)		E_p=30 MeV $E^* \pm \Delta E$ (keV)		E_p=35 MeV $E^* \pm \Delta E$ (keV)		E_p=40 MeV $E^* \pm \Delta E$ (keV)		All Energies $E^* \pm \Delta E$ (keV)	
3736	1	3736	1	3736	1	3736	1	3736	1
3903	1	3902	1	3904	1	3904	1	3903	1
4490	2	4491	1	4491	1	4491	1	4491	1
5261	7	5261	5	5265	5	5264	5	5263	6
5617	3	5618	2	5617	4	5618	4	5617	3
5901	5	5904	1	5904	2	5901	5	5902	4
6026	3	6026	3	6027	2	6026	3	6026	3
6286	1	6284	2	6285	1	6285	1	6285	1
6499	6	6505	5	6510	4	6508	3	6505	6
6580	2	6582	2	6582	3	6582	2	6581	2
6750	4	6752	2	6751	4	6752	5	6751	4
6929	4	6927	6	6924	5	6923	3	6926	5
7114	1	7115	2	7113	1	7114	1	7114	1
7455	3	7453	5	7456	4	7458	6	7455	5
7540	5	7542	5	7545	1	7546	3	7543	5
7671	8	7676	9	7672	1	7673	7	7673	8
7867	4	7868	5	7871	1	7871	2	7869	4
7919	6	7923	4	7924	2	7927	5	7923	6
8097	6	8100	5	8102	3	8100	3	8100	5
8360	7	8366	3	8370	2	8368	5	8366	6
8416	6	8419	4	8420	4	8419	3	8418	4
8563	5	8565	5	8566	4	8564	7	8564	6
8741	7	8750	3	8749	2	8748	5	8747	6
8849	6	8851	3	8849	3	8849	4	8850	4
				8978	6			8978	6
				9029	5			9029	5
				9145	5			9145	5
				9237	3			9237	3
				9360	5			9360	5
				9413	5			9413	5
				9591	4			9591	4
				9642	6			9642	6
				9859	4			9859	4
				10051	3			10051	3
				10277	3			10277	3

Table V. Optical Parameters

r_R = 1.16 F,		a_R = 0.75 F	
r_I = 1.37 F,		a_I = 0.63 F	
r_{SO} = 1.064 F		a_{SO} = 0.738 F	
V_{SO} = 6.04 MeV		r_C = 1.25 F	
E_p(MeV)	V_0(MeV)	W_0(MeV)	W_D(MeV)	χ^2
25	48.92	2.10	4.07	3.60
30	47.86	2.40	4.18	1.90
35	46.42	2.37	4.17	6.87
40	44.51	1.71	4.42	4.28

Table VI. Deformations as a Function of Beam Energy for ^{40}Ca

E*(keV)	L	δ_L (F) E_p=24.93 MeV	E_p=30.04 MeV	E_p=34.78 MeV	E_p=39.83 MeV
3736	3	1.40	1.38	1.35	1.32
3903	2	0.42	0.43	0.42	0.43
4491	5	0.91	0.86	0.83	0.80
5249	2	0.15	0.14	0.12	0.12
5279	4	0.16	0.15	0.14	0.13
5617	5	0.42	0.36	0.33	0.31
6026	3	0.23	0.20	0.18	0.17
6285	3	0.46	0.43	0.41	0.40
6505	4	0.18	0.17	0.18	0.17
6581	3	0.41	0.36	0.33	0.32
6751	3	0.27	0.24	0.22	0.21
6909	2	0.44	0.43	0.42	0.45
7114	5	0.40	0.32	0.29	0.27
7292	2	0.10	0.10	0.09	0.09
7455	4	0.20	0.17	0.16	0.15
7531	3	0.19	0.17	0.17	0.15
7558	4	0.23	0.20	0.20	0.19
7869	2	0.28	0.25	0.23	0.23
7923	4	0.34	0.31	0.29	0.29
8092	2	0.18	0.17	0.17	0.16
8113	3	0.19	0.17	0.16	0.15
8191	6	0.22		0.15	
8366	4	0.32	0.31	0.31	0.33
8418	3	0.29	0.27	0.25	0.25
8535	5	0.23	0.20	0.19	0.18
8578	2	0.18	0.17	0.17	0.17
8747	2	0.17	0.15	0.15	0.14
8850	7	0.10	0.10	0.09	0.09
8978	6			0.17	0.15
9029	5			0.16	0.15
9145	3			0.23	
9237	7			0.06	
9360	3			0.16	
9413	3			0.26	
9541	4			0.15	
9591	3			0.12	
9859	5			0.19	
10051	5			0.19	
10277	4			0.18	

Table VII. Reduced Transition Probabilities in Single-Particle Weisskopf Units, "mass-transport" Parameters, and "force constants" for ^{40}Ca

E*(keV)	L	G_{sp}	$B_L/\hbar^2$ (MeV)$^{-1}$		C_L (MeV)	
3736	3	26.6	0.11	2	0.15	3
3903	2	2.1	0.74	2	0.11	4
4491	5	17.2	0.37	2	0.75	3
5249	2	0.2	0.70	3	0.19	5
5279	4	0.4	0.97	3	0.27	5
5617	5	2.6	0.19	3	0.61	4
6026	3	0.5	0.36	3	0.13	5
6285	3	2.4	0.69	2	0.27	4
6505	4	0.6	0.45	3	0.19	5
6581	3	1.6	0.99	2	0.43	4
6751	3	0.7	0.22	3	0.99	4
6909	2	2.1	0.42	2	0.20	4
7114	5	2.0	0.20	3	0.99	4
7292	2	0.1	0.86	3	0.46	5
7455	4	0.5	0.50	3	0.28	5
7531	3	0.4	0.35	3	0.20	5
7558	4	0.8	0.31	3	0.18	5
7869	2	0.6	0.13	3	0.80	4
7923	4	1.6	0.14	3	0.88	4
8092	2	0.3	0.23	3	0.15	5
8113	3	0.4	0.36	3	0.24	5
8191	6	0.7	0.77	3	0.52	5
8366	4	1.9	0.11	3	0.80	4
8418	3	0.9	0.14	3	0.98	4
8535	5	0.9	0.39	3	0.28	5
8578	2	0.3	0.22	3	0.16	5
8747	2	0.3	0.27	3	0.21	5
8850	7	0.4	0.21	4	0.17	6
8978	6	1.0	0.52	3	0.42	5
9029	5	0.6	0.51	3	0.41	5
9145	3	0.8	0.15	3	0.12	5
9237	7	0.2	0.48	4	0.41	6
9360	3	0.4	0.29	3	0.26	5
9413	3	1.0	0.12	3	0.10	5
9541	4	0.4	0.43	3	0.40	5
9591	3	0.2	0.50	3	0.46	5
9859	5	0.9	0.32	3	0.31	5
10051	5	0.9	0.30	3	0.30	5
10277	4	0.6	0.27	3	0.29	5

Table VIII. Fraction of Sum Rules Exhausted for ^{40}Ca at 35 MeV

E*(keV)	L	EWSR	NEWSR
3736	3	0.221	0.538
3903	2	0.032	0.058
4491	5	0.064	0.187
5249	2	0.003	0.005
5279	4	0.002	0.005
5617	5	0.012	0.029
6026	3	0.007	0.010
6285	3	0.034	0.049
6505	4	0.005	0.009
6581	3	0.024	0.033
6751	3	0.011	0.015
6909	2	0.057	0.058
7114	5	0.012	0.022
7292	2	0.003	0.003
7455	4	0.005	0.007
7531	3	0.007	0.008
7558	4	0.008	0.011
7869	2	0.018	0.017
7923	4	0.017	0.024
8092	2	0.010	0.009
8113	3	0.007	0.007
8191	6	0.008	0.006
8366	4	0.021	0.028
8418	3	0.017	0.018
8535	5	0.006	0.009
8578	2	0.011	0.009
8747	2	0.009	0.007
8850	7	0.001	0.002
8978	6	0.005	0.008
9029	5	0.005	0.007
9145	3	0.016	0.016
9237	7	0.001	0.001
9360	3	0.008	0.008
9413	3	0.020	0.020
9541	4	0.005	0.006
9591	3	0.005	0.004
9859	5	0.007	0.010
10051	5	0.008	0.010
10277	4	0.009	0.009

Table IX. Ratio of Total Cross-Sections σ[D+E]/σ[D]

E_p	3^-		5^-	
(MeV)	Schaeffer[a]	This Work*	Schaeffer[a]	This Work*
17.3	2.7		6.8	
20.3	3.3		7.9	
25.0		3.5		7.8
30.0	2.9	3.1	6.4	6.4
35.0		2.8		5.5
40.0	2.5	2.5	4.6	4.8
50.0	2.3		3.6	

[a]Ref. 39

able X. Spin and Parity Assignments of States in ^{40}Ca

			(p,p')			(α,α')		(e,e')		(^{3}He,d)		(d,n)	(p,γ)		(p,p'γ)				γ-Res	
			25-40 MeV	55 MeV	17 MeV	51 MeV	31 MeV	120-220 MeV	20-60 MeV	12 MeV	14 MeV	6 MeV			7.9-9.6 MeV	9 MeV	8-10 MeV	12 MeV		Probable Assign.
Ref. a	b		b	c	d	e	f	g	h	i	j	k	l	m	n	o	p	q	r	
E*(keV)	E*±ΔE(keV)		L	L	L	J^π	J^π	J^π	J^π	J^π	J^π	J^π	J^π	J^π	J^π	J^π	J^π	J^π	J^π	J^π
3350	3350														0^+	0^+	0^+			0^+
3737	3736	1	3	3	3	3^-	3^-	3^-	3^-	3^-	3^-	3^-	3^-	3^-	3^-	3^-	3^-			3^-
3904	3903	1	2		2	2^+	2^+	2^+	2^+				2^+	2^+	2^+	2^+	2^+			2^+
4492	4491	1	5	5		5^-	5^-	5^-		5^-	5^-	5^-	5^-	5^-	5^-	5^-	5^-			5^-
5212															0,(1)	0^+	0^+			0^+
5249	5263	6	2										2	2	2	2^+	2^+			2^+
5279			4			$()^-$							4^+	4^+	4	4^+	4^+			4^+
5615	5617	3	5			$()^-$	(2^+)			4^-	4^-	4^-	4^-	4^-	$4^{(-)}$	4^-	4^-			4^-
5627														2	2	2^+	2^+			2^+
5900	5902	4	1			3^-	1^-			1^-	1^-	1^-			1^-	1^-	1^-			1^-
6025	6026	3	3							(2^-)	(2^-)	$(2,3)^-$			3,(2)	2^-	2^-			2^-
6029																3^+	3^+	(3^+)		(3^+)
6285	6285	1	3		3	3^-	3^-	3^-		3^-	3^-	3^-	3^-		3^-	3^-	3^-			3^-
6509	6505	6	4														4^+			4^+
6544					3												4^+			4^+
6585	6581	2	3			3^-	3^-			(3^-)	3^-	3^-					3^-			3^-
6750	6751	4	3							$()^-$	$(2,0)^-$	$(2)^-$			$(3)^-$					$(2)^-$
6909	6909	5	2			$2^+ + 3^-$	(2^+)											(2^+)	2^+	2^+
6930			(≥3)	2+3	2	$2^+ + 1^-$		$(2^+ + 3^-)$	$(2^+ + 3^-)$				(1,2)					(3^-)		(3^-)
6948	6948	5	1				1^-			$()^-$	1^-	1^-						(1^-)	1^-	1^-
7114	7114	1	5		3					$()^-$	$(3)^-$	3^-						$(2^+),(3^-)$		?
7280	7292	5	(0,2)										0					0^+		(0^+)
7300																				(4^+)
7455	7455	5	4											2				(2^+)		(2^+)
7473																				
7531	7543	5	3								$(2)^-$	$(2)^-$								$(2)^-$
7558			(4)											<5						(4^+)
7655										4^-	4^-									4^-
7676	7673	8	(≥6)																	(≥6)
7696										$(3)^-$	3^-									3^-
7867	7869	4	2				(2^+)											(2^+)		2^+
7928	7923	6	4			4^+	4^+													4^+
8092	8100	5	2			2^+	2^+											(2^+)		2^+
8113			3															(1^-)		$(1,2,3)^-$
8186	8191	5	(6)																	(6^+)
8271	8274	6	1				(2^+)											$(0^-),(2^+)$		$(0^-,2^+)$
8371	8366	6	4			4^+	4^+													4^+
8424	8418	4	3							(2^-)	2^-	2^-								2^-
8535	8564	6	5			2^+		5^-		(5^-)	5^-	5^-								5^-
8578			2															(2^+)		2^+
8743	8747	6	2															(1^-)		$(1^-,2^+)$
8848	8850	4	7																	(6^-)
8977	8978	6	6																	(6^+)
8993																		(2^+)		2^+
9028	9029	5	5																	
9132	9145	5	3																	
9158																				(6^-)
	9237	3	7																	
	9360	5	3																	
	9413	5	3									$(3)^-,(2)^-$	2							$(3)^-,(2)^-$
	9541	5	4										1^-							
	9591	4	3																	2^-
	9642	6											2^-							
	9859	4	5										1							
	10051	3	5									$(0)^-$								
	10277	3	4																	

Table XI. Deformed State Calculations of Gerace and Green

Main Configuration	0^+	2^+	4^+
4p-4h (mixed with 2p-2h)	3.55 MeV	3.90	5.25
2p-2h (mixed with 4p-4h)	7.33 MeV	6.90	8.00

Table XII. Comparison of Nuclear Deformations, $\delta_L(F)$.

E^* (MeV)	L	(p,p') this experiment		(p,p') [a]	(p,p') [b]	(α,α') [c]	(α,α') [d]	(e,e') [e]
		40 MeV	25 MeV	17 MeV	55 MeV	50 MeV	31 MeV	120-220 MeV
3.736	3	1.32	1.40	1.44	1.32	0.85	0.96	0.84
3.903	2	0.43	0.42	0.40		0.34	0.40	0.48
4.491	5	0.80	0.91		0.68	0.35	0.52	0.40
6.285	3	0.40	0.46	0.52		0.40	0.48	0.23
6.581	3	0.32	0.41	0.60		0.31	0.36	
7.114	5	0.27	0.40	0.68*				
7.869	2	0.23	0.28				0.32	
7.923	4	0.29	0.34			0.29	0.36	0.40
8.366	4	0.32	0.32			0.24	0.32	
8.535	5	0.18	0.23					0.31
8.578	2	0.14	0.17			0.19		

[a] Ref. 65
[b] Ref. 66
[c] Ref. 8
[d] Ref. 7
[e] Ref. 9
*L=3 was used

Table XIII. Comparisons of Reduced Transition Probabilities, G(sp) in Weisskopf Single Particle Units.

Transition (100% or 100%)		(p,p') Present 40 MeV	(e,e') a	(e,e') b		(p,p'γ) e	(p,p'γ) f	(p,p'γ) g
3^-(3.736)	0^+(g.s.)	28.7 ±2.0	31.7	7.4±0.8		20.7 ±5.1		
2^+(3.903)	"	2.05±0.2	2.0	2.4±0.75	4±1.3[c]	2.47±0.82	1.6±0.5	1.7
2^+(5.429)	"	0.26±0.05				0.12±0.02		1.1
2^+(6.909)	"	2.25±0.23	1.7	2.7±0.3	1.7[d]		1.7±0.15	4

[a] Ref. 10
[b] Ref. 9
[c] Ref. 55
[d] Ref. 59
[e] Ref. 26
[f] Ref. 50
[g] Ref. 67

*Fermi Equivalent, uniform charge distribution with r_o=1.33F.

Table XIV. Comparisons of Reduced Transition Probabilities Between (p,p') and (α,α')

E^* (MeV)	L	G_L (Single Particle Units) (p,p') this work	G_L (Single Particle Units) $(\alpha,\alpha')^a$
3.90	2	2.05 ± 0.20	2.9 ± 0.5
5.62	2	0.13 ± 0.05	0.7 ± 0.2
7.87	2	0.92 ± 0.15	1.8 ± 0.4
8.10	2	0.38 ± 0.06	2.1 ± 0.3
3.73	3	28.7 ± 3.0	23.6 ± 3.5
6.29	3	3.1 ± 0.3	6.6 ± 1.0
6.58	3	2.5 ± 0.3	3.8 ± 0.6
7.94	4	2.2 ± 0.2	5.6 ± 0.8
8.38	4	2.0 ± 0.2	4.3 ± 0.6
4.49	5	20.6 ± 2.1	17.7 ± 2.7

[a] Reference 7

Also in Advances in Nuclear Physics, edited by M. Baranger and E. Vogt (Plenum Press, Inc. New York), Vol. III.

FIGURE CAPTIONS

1. $^{40}Ca(p,p')^{40}Ca^*$ spectrum taken at $\theta_{LAB}=31.7°$ for $E_p=39.83$ MeV.
2. $^{40}Ca(p,p')^{40}Ca^*$ spectrum taken at $\theta_{LAB}=31.2°$ for $E_p=34.78$ MeV.
3. $^{40}Ca(p,p')^{40}Ca^*$ spectrum taken at $\theta_{LAB}=31.7°$ for $E_p=30.04$ MeV.
4. $^{40}Ca(p,p')^{40}Ca^*$ spectrum taken at $\theta_{LAB}=31.7°$ for $E_p=24.93$ MeV.
5. Optical model fits to the experimental elastic scattering results at $E_p=25$ to 40 MeV.
6. The decomposition of doublet at $E_x=8.558$ MeV.
7. The decomposition of doublet at $E_x=7.539$ MeV.
8. The decomposition of doublet at $E_x=8.097$ MeV.
9. Spectrum fits using two superimposed standard peaks for the analysis of 6.909, 6.930, 6.948 triplet.
10. Summary of the DWBA calculations using collective model F.F. for L=2 to L=8 at $E_p=25$ to 40 MeV.
11. Experimental distributions of L=2 states and collective model fits (solid curves). The dash curves are those of 3.903 MeV state.
12. Experimental distribution of L=3 states and collective model fits (solid curves). The dash curves are those of 3.736 MeV state.
13. Experimental distrubitions of L=4 states. Solid curves are collective model fits. Dash curves are those of 6.505 state.

14. Experimental distribution of L=5 states and collective model fits (solid curves). The dash curves are those of 4.491 MeV state.
15. Experimental distributions of L=6 and L=7 states, and collective model fits (solid curves).
16. Experimental distributions of L=1 states. The solid curves show the poor collective model predictions.
17. Results of generalized collective model calculations for the 0^+ excitation.
18. The empirical form factor used in fitting the data. The solid curves are DWBA calculations using the empirical form factor and are shown in comparisen with the data.
19. Theoretical and experimental energy levels for negative parity states of ^{40}Ca.
20. Microscopic DWBA calculations for the 1^-, T=0 state.
21. Microscopic DWBA calculations for the 1st 3^-, T=0 state.
22. Microscopic DWBA calculations for the 2nd 3^-, T=0 state.
23. Microscopic DWBA calculations for the 1st 5^-, T=0 state.
24. Microscopic DWBA calculations for the 1st 2^-, T=0 state.
25. Microscopic DWBA calculations for the 3rd 3^-, T=0; 1st 3^-, T=1; 1st 4^-, T=0,1; 1st 4^-, T=1; and 6^- T=0, 1 states.
26. Systematics of the even-parity states in ^{40}Ca observed in this experiment. Open circles are those from other experiments.
27. Energy levels of ^{40}Ca observed by various experiments.

Fig. 1

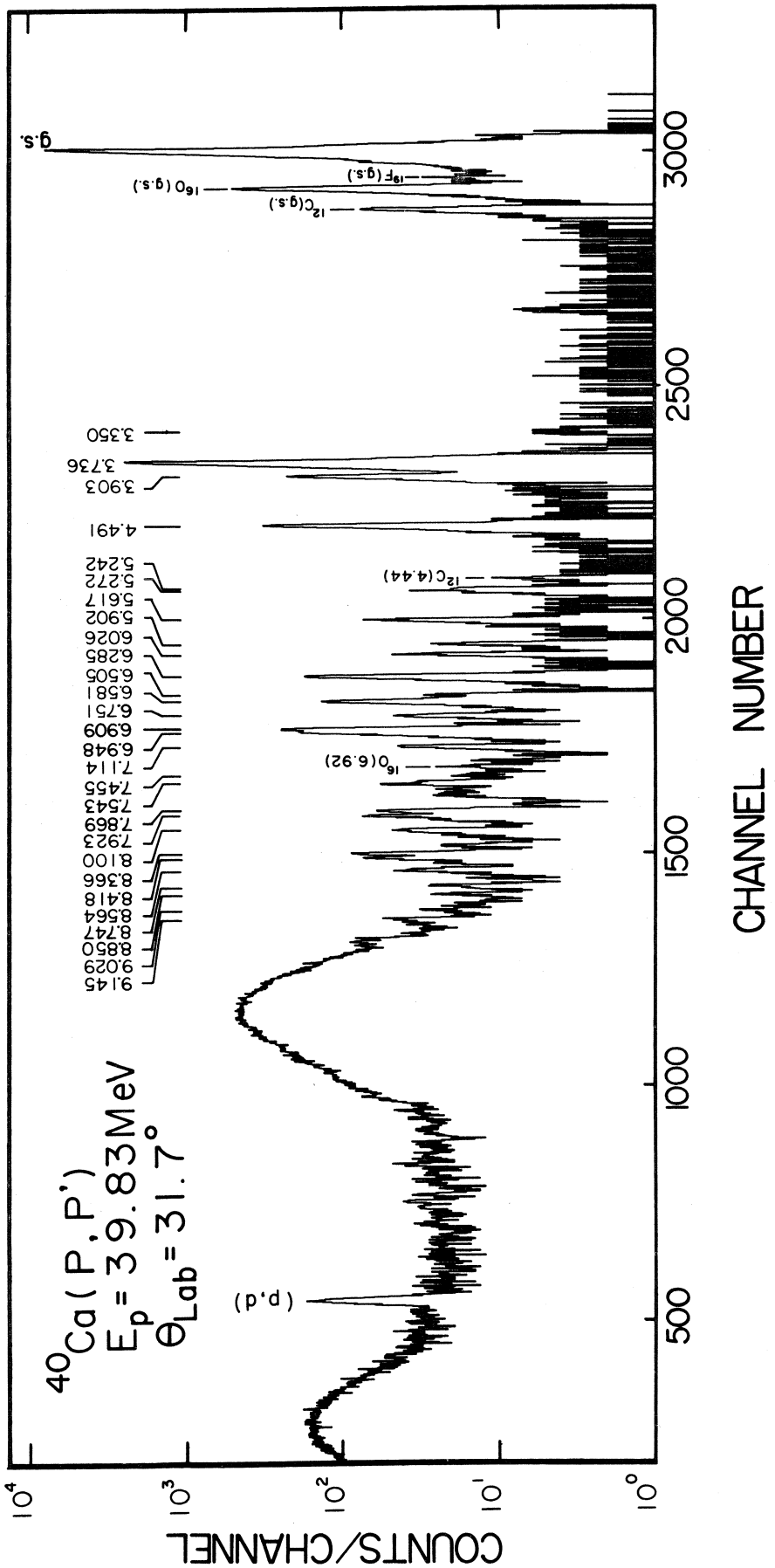
$^{40}Ca(P,P')$
$E_p = 39.83$ MeV
$\theta_{Lab} = 31.7°$
(p,d)
$^{16}O(6.92)$
$^{12}C(4.44)$
$^{12}C(g.s.)$
^{16}O (g.s.)
^{19}F (g.s.)
g.s.
9.145
9.029
8850
8.747
8564
8.418
8.366
8100
7.923
7.869
7.543
7.455
7.114
6.948
6.909
6.751
6581
6.505
6.285
6026
5.902
5.617
5.272
5.242
4.491
3.903
3.736
3.350
COUNTS/CHANNEL
CHANNEL NUMBER
500
1000
1500
2000
2500
3000

Fig. 2

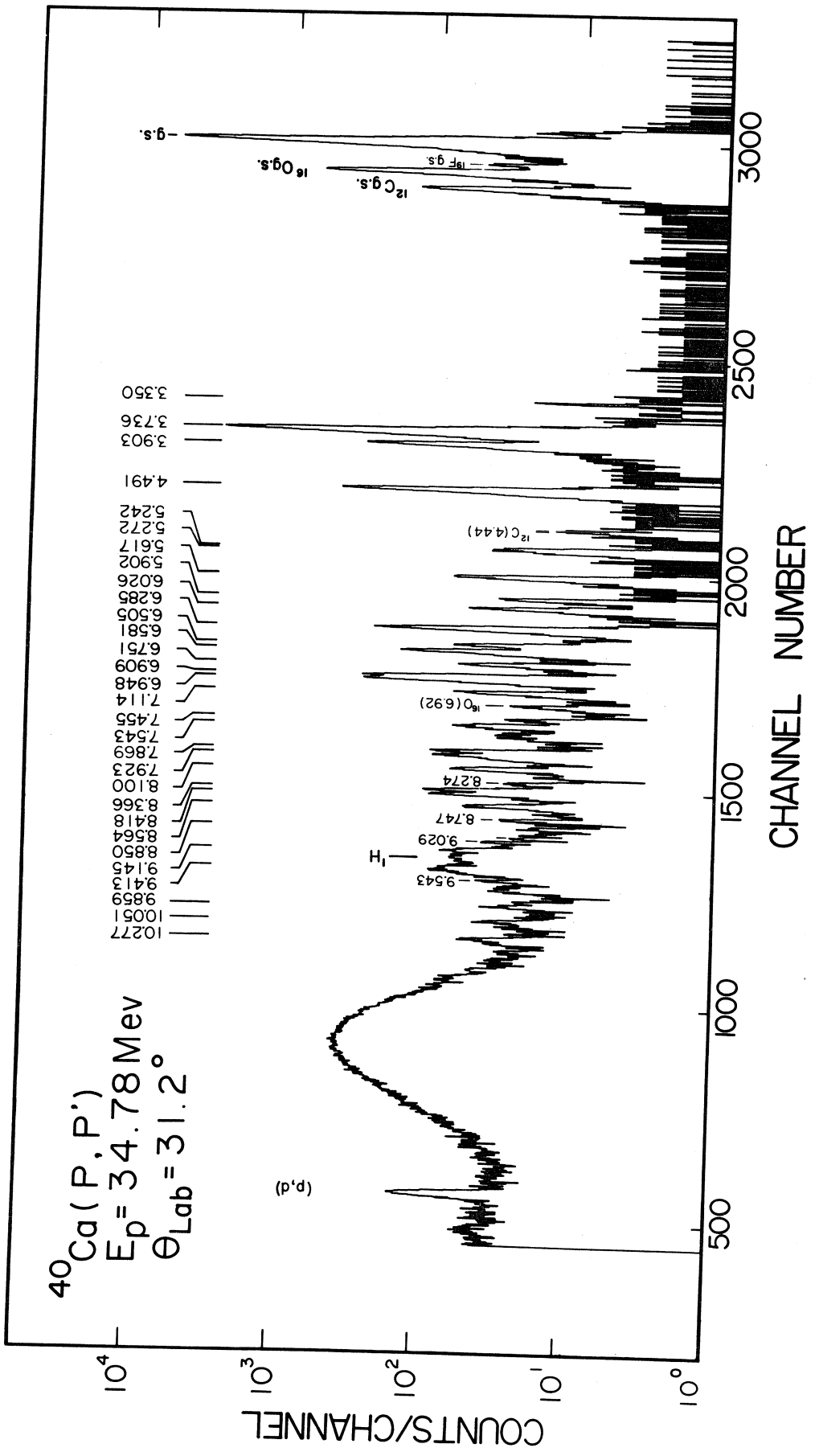
40Ca(P,P')
Ep= 34.78 Mev
θLab= 31.2°
COUNTS/CHANNEL
CHANNEL NUMBER
(p,d)
1H
9.543
9.029
8.747
8.274
16O(6.92)
12C(4.44)
12C g.s.
16O g.s.
19F g.s.
g.s.
3.350
3.736
3.903
4.491
5.242
5.272
5.617
5.902
6.026
6.285
6.505
6.581
6.751
6.909
6.948
7.114
7.455
7.543
7.869
7.923
8.100
8.366
8.418
8.564
8.850
9.145
9.413
9.859
10.051
10.277

Fig. 3

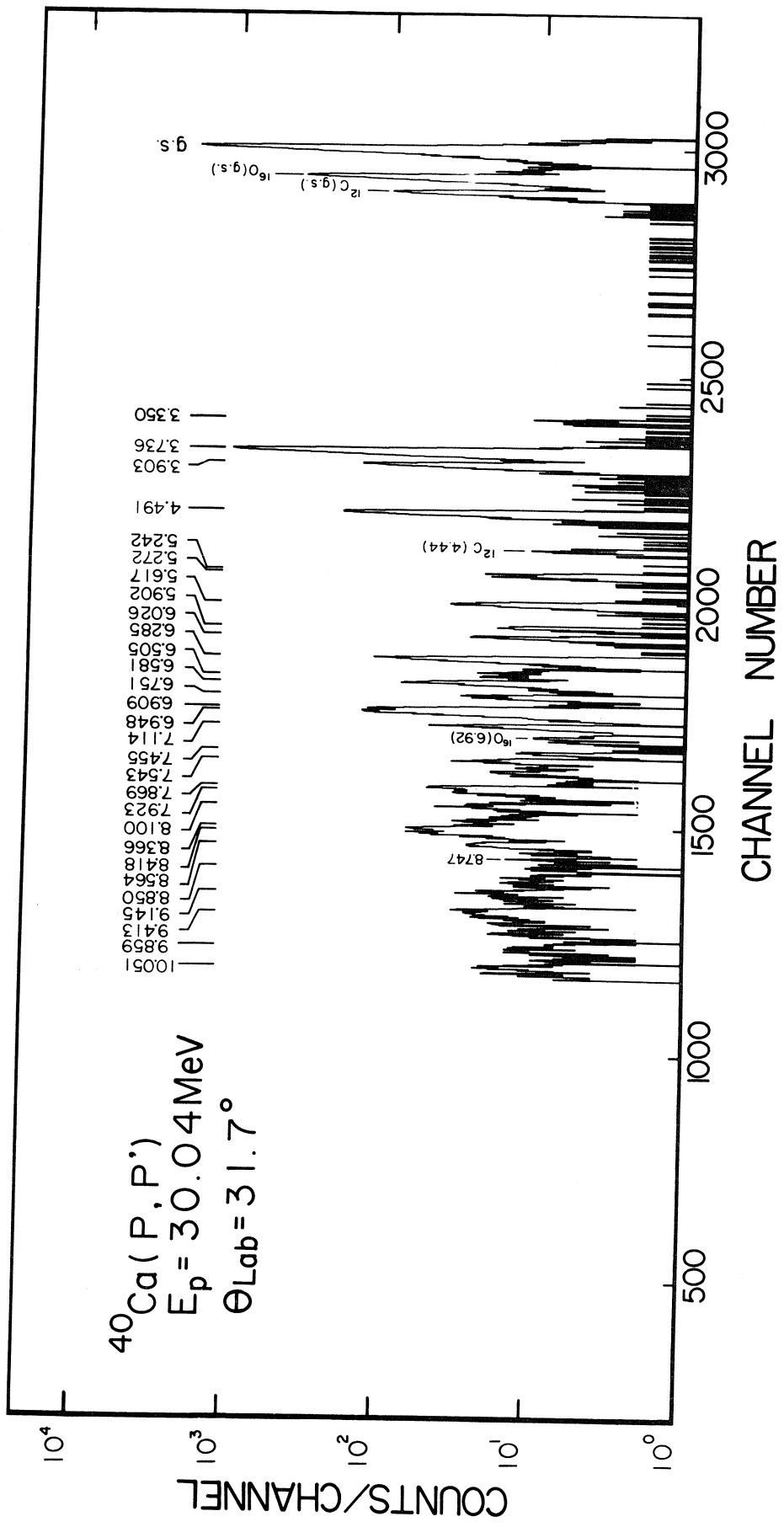
COUNTS/CHANNEL
CHANNEL NUMBER
$^{40}Ca(P,P')$
$E_p = 30.04$MeV
$\theta_{Lab} = 31.7°$
g.s.
^{16}O(g.s.)
^{12}C(g.s.)
^{16}O(6.92)
^{12}C(4.44)
8.747
10.051
9.859
9.413
9.145
8.850
8.564
8.418
8.366
8.100
7.923
7.869
7.543
7.455
7.114
6.948
6.909
6.751
6.581
6.505
6.285
6.026
5.902
5.617
5.272
5.242
4.491
3.903
3.736
3.350

Fig. 4

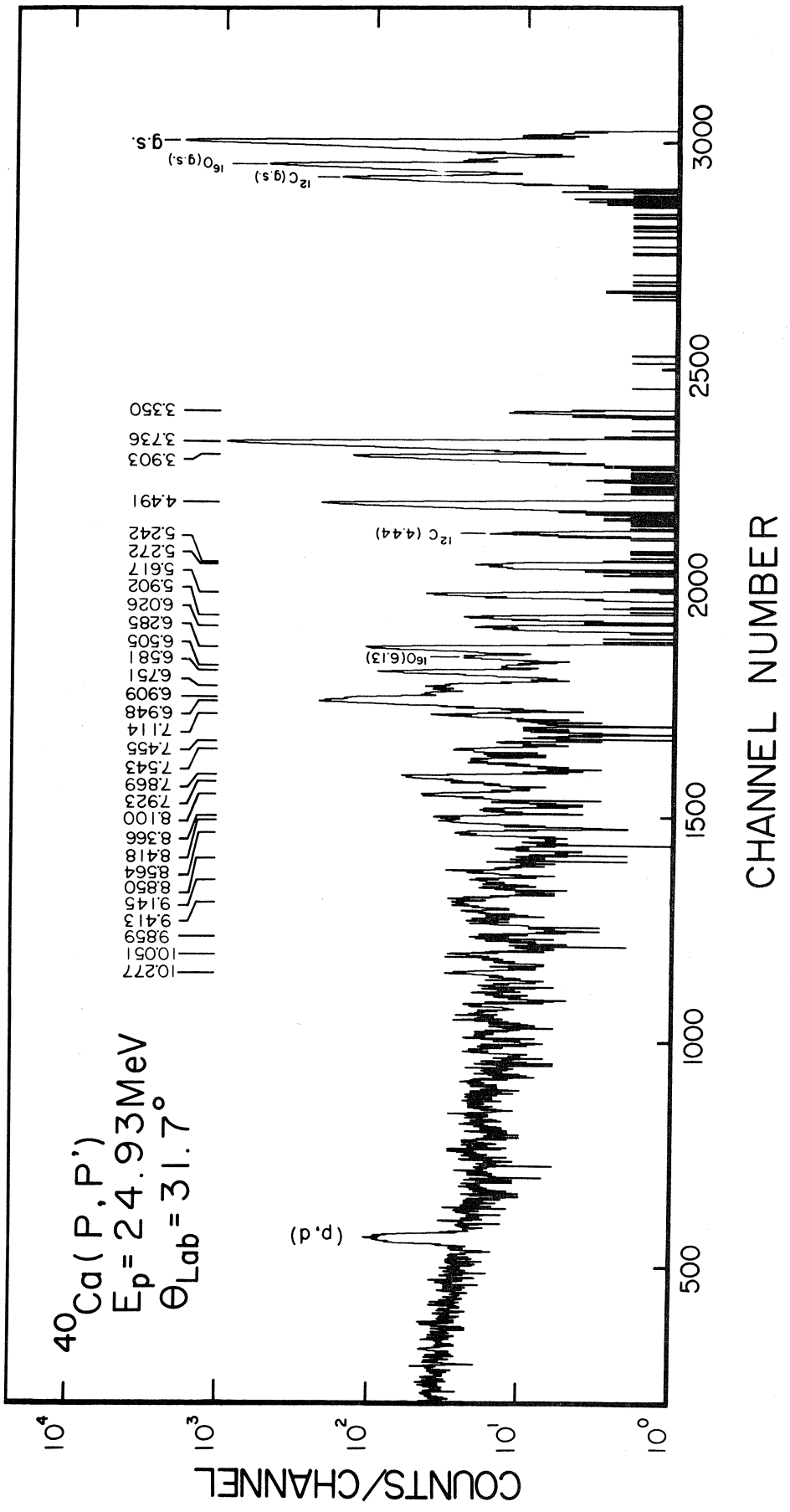
COUNTS/CHANNEL
CHANNEL NUMBER
$^{40}Ca(P,P')$
$E_p = 24.93MeV$
$\theta_{Lab} = 31.7°$
(p,d)
$^{16}O(6.13)$
^{12}C (4.44)
^{12}C(g.s.)
^{16}O(g.s.)
g.s.
10.277
10.051
9.859
9.413
9.145
8.850
8.564
8.418
8.366
8.100
7.923
7.869
7.543
7.455
7.114
6.948
6.909
6.751
6.581
6.505
6.285
6.026
5.902
5.617
5.272
5.242
4.491
3.903
3.736
3.350

Fig. 5

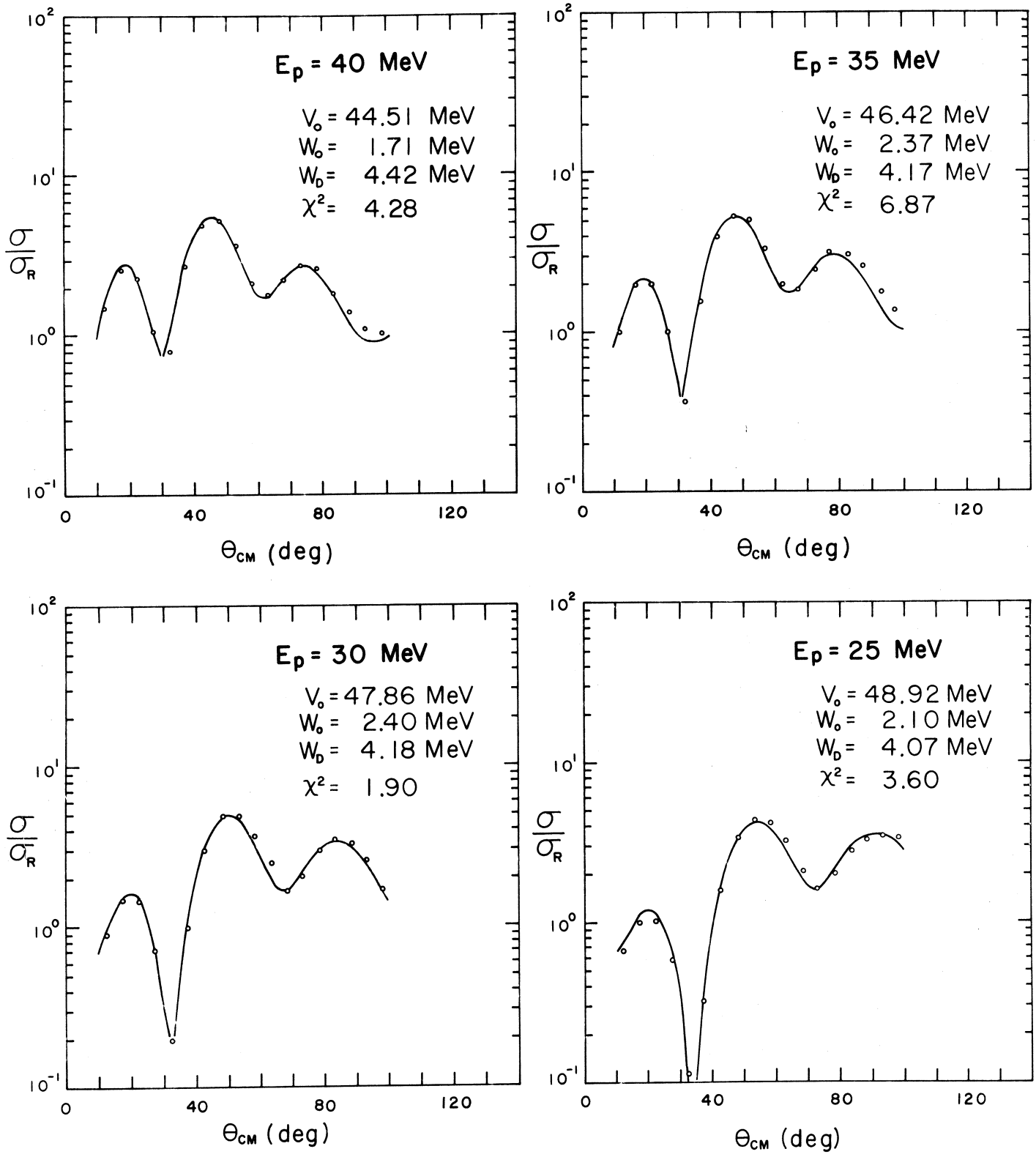
E_p = 40 MeV
V_o = 44.51 MeV
W_o = 1.71 MeV
W_D = 4.42 MeV
χ^2 = 4.28
E_p = 35 MeV
V_o = 46.42 MeV
W_o = 2.37 MeV
W_D = 4.17 MeV
χ^2 = 6.87
E_p = 30 MeV
V_o = 47.86 MeV
W_o = 2.40 MeV
W_D = 4.18 MeV
χ^2 = 1.90
E_p = 25 MeV
V_o = 48.92 MeV
W_o = 2.10 MeV
W_D = 4.07 MeV
χ^2 = 3.60
$\frac{\sigma}{\sigma_R}$
θ_{CM} (deg)
10^2
10^1
10^0
10^{-1}
0
40
80
120

Fig. 6

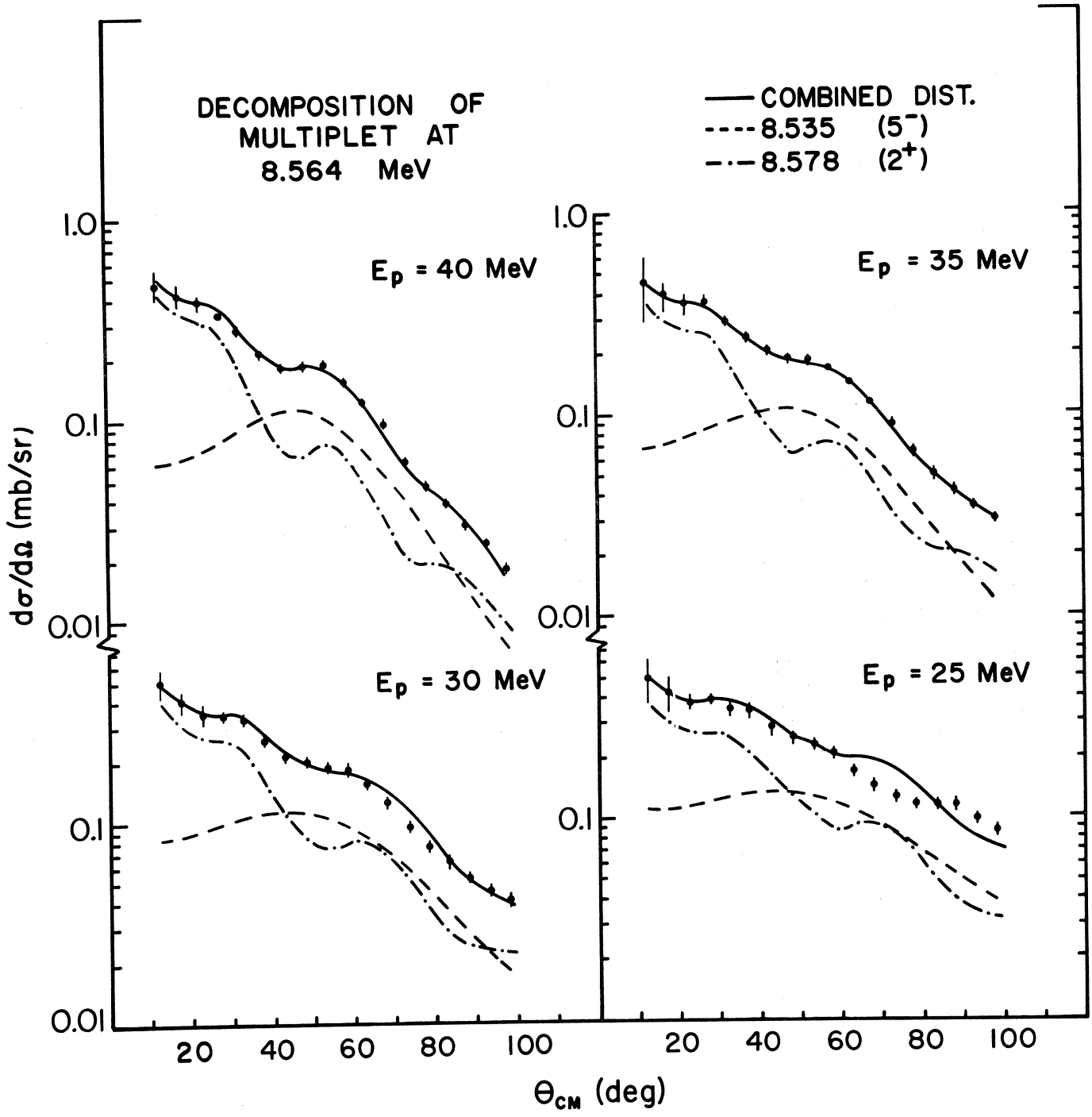
DECOMPOSITION OF MULTIPLET AT 8.564 MeV
COMBINED DIST.
8.535 (5⁻)
8.578 (2⁺)
Ep = 40 MeV
Ep = 35 MeV
Ep = 30 MeV
Ep = 25 MeV
dσ/dΩ (mb/sr)
1.0
0.1
0.01
20
40
60
80
100
θcm (deg)

Fig. 7

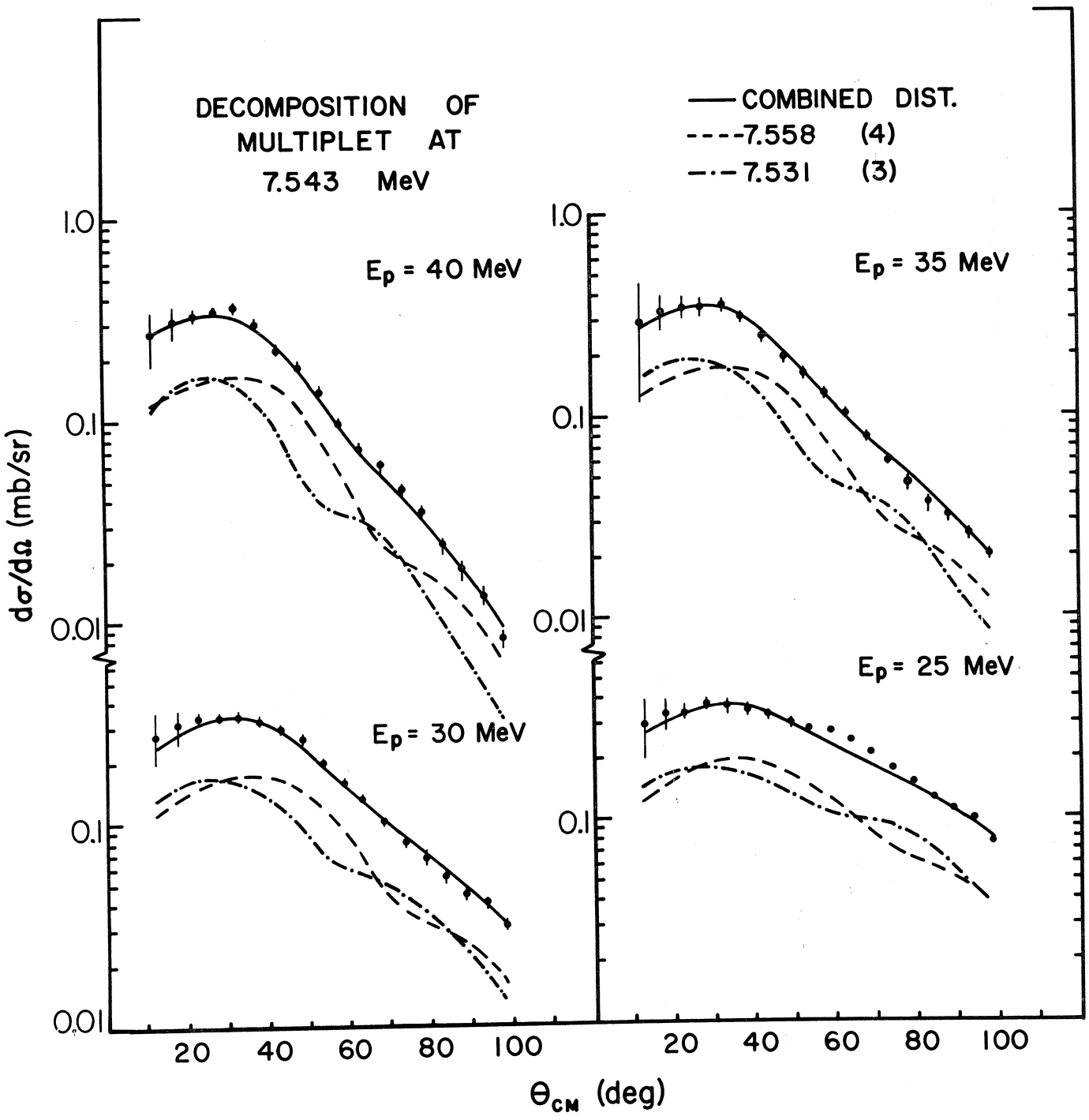
DECOMPOSITION OF MULTIPLET AT 7.543 MeV
COMBINED DIST.
7.558 (4)
7.531 (3)
Ep = 40 MeV
Ep = 35 MeV
Ep = 30 MeV
Ep = 25 MeV
dσ/dΩ (mb/sr)
1.0
0.1
0.01
20
40
60
80
100
θcm (deg)

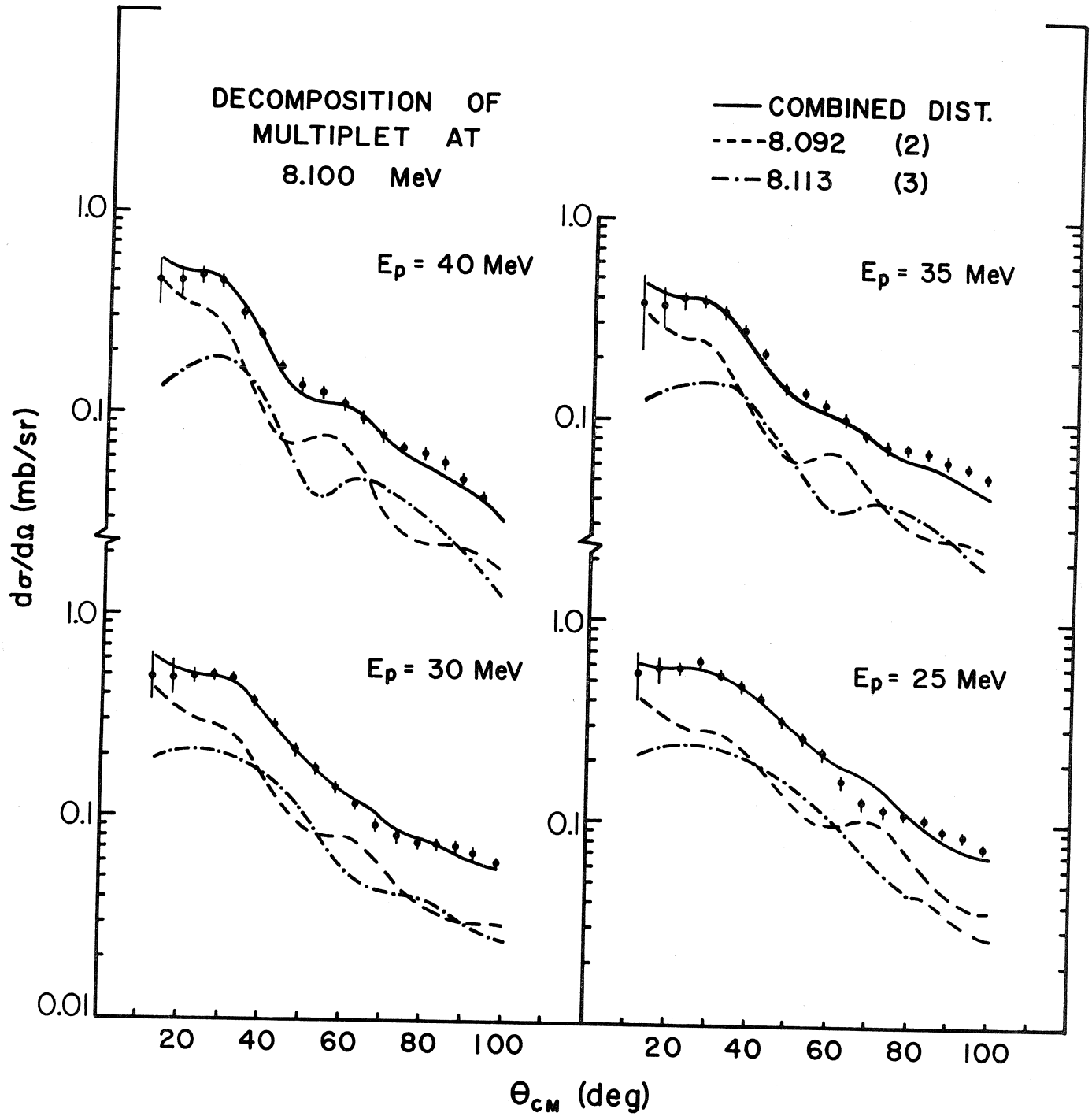
DECOMPOSITION OF
MULTIPLET AT
8.100 MeV
COMBINED DIST.
8.092 (2)
8.113 (3)
Ep = 40 MeV
Ep = 35 MeV
Ep = 30 MeV
Ep = 25 MeV
dσ/dΩ (mb/sr)
1.0
0.1
0.01
20
40
60
80
100
θcm (deg)

Fig. 9

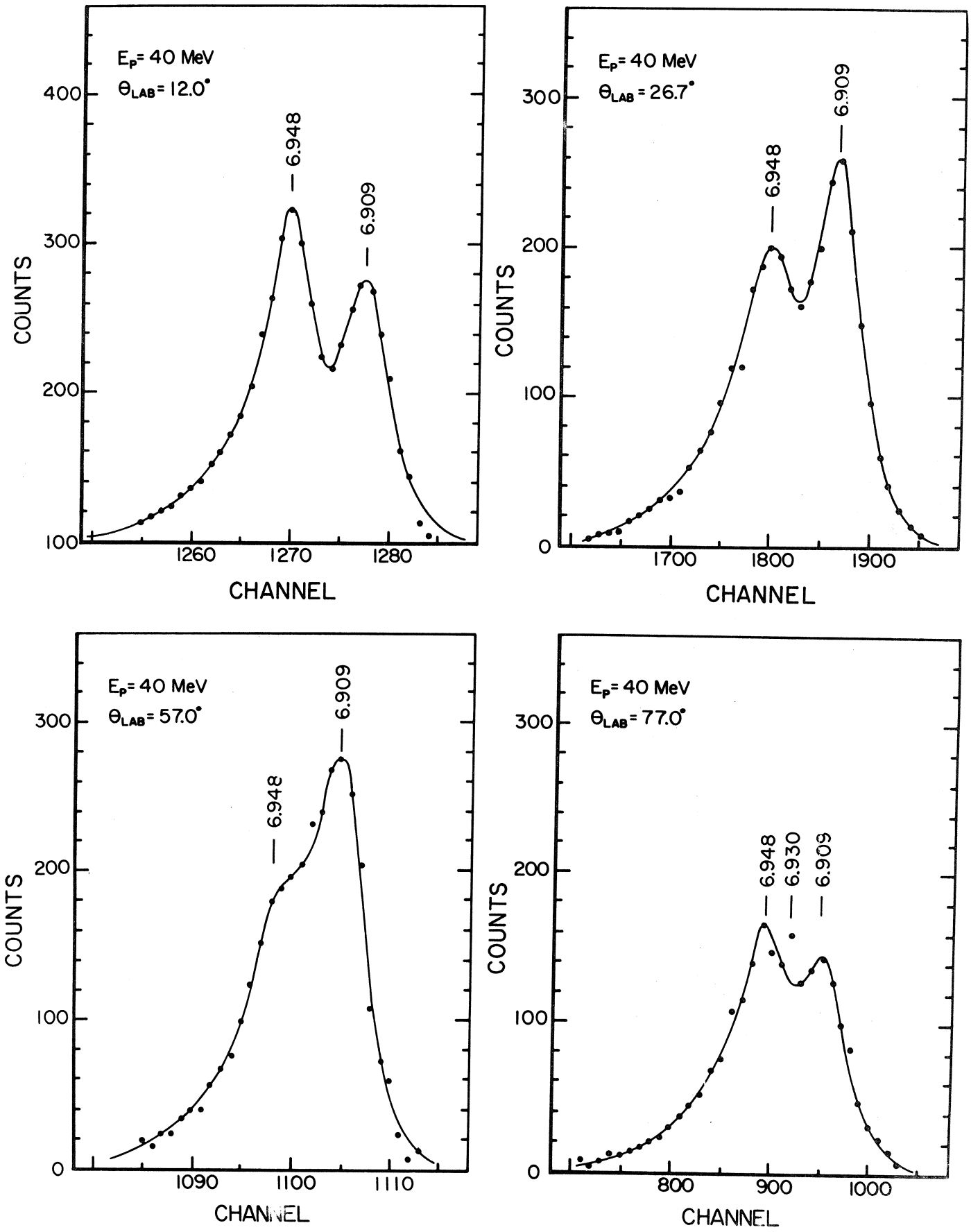
E_p= 40 MeV
θ_{LAB}= 12.0°
6.948
6.909
COUNTS
CHANNEL
E_p= 40 MeV
θ_{LAB}= 26.7°
6.948
6.909
COUNTS
CHANNEL
E_p= 40 MeV
θ_{LAB}= 57.0°
6.948
6.909
COUNTS
CHANNEL
E_p= 40 MeV
θ_{LAB}= 77.0°
6.948
6.930
6.909
COUNTS
CHANNEL

Fig. 10

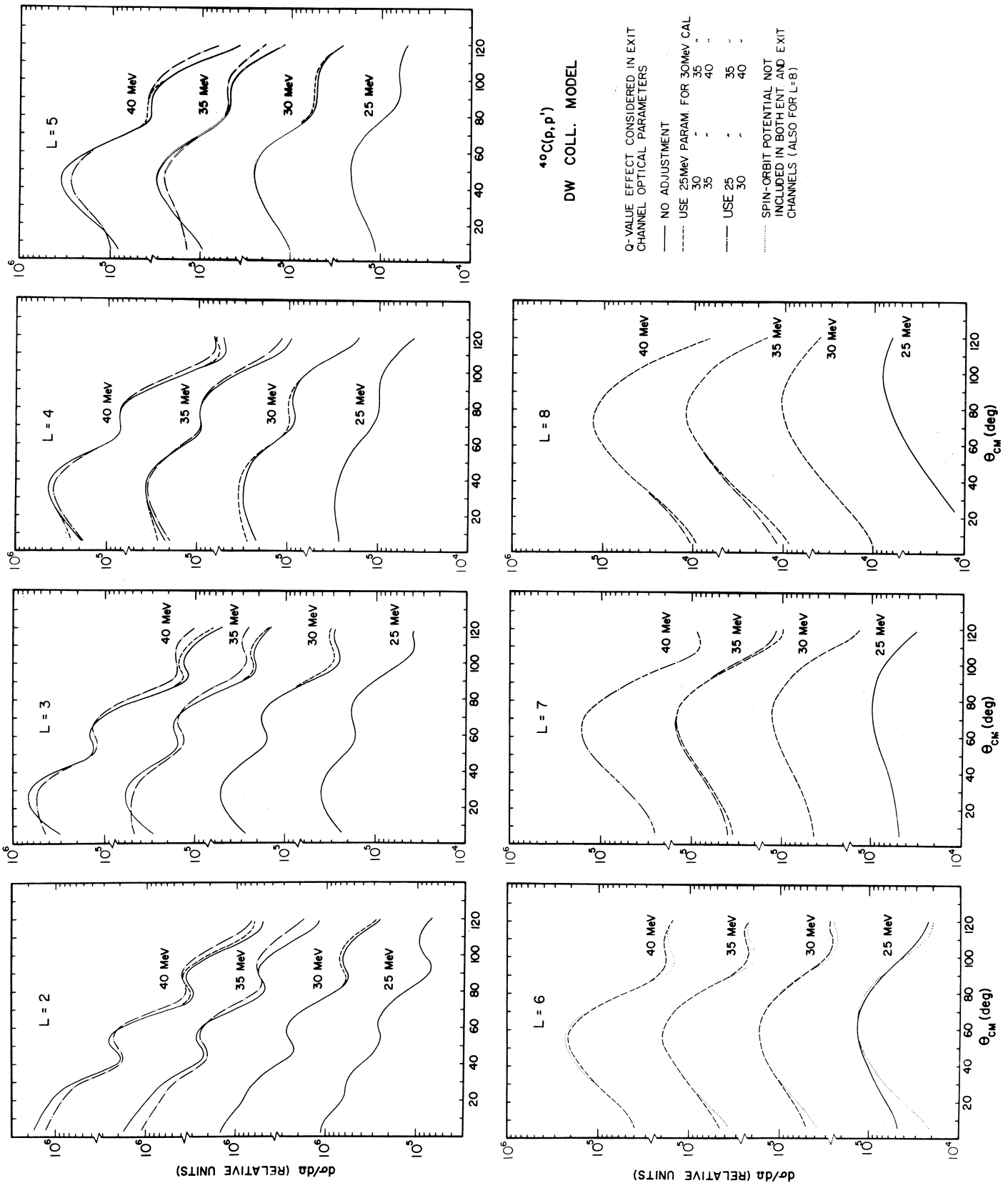
$^{40}C(p,p')$
DW COLL. MODEL
Q-VALUE EFFECT CONSIDERED IN EXIT CHANNEL OPTICAL PARAMETERS
NO ADJUSTMENT
USE 25MeV PARAM. FOR 30MeV CAL
30 " 35 "
35 " 40 "
USE 25 " 35 "
30 " 40 "
SPIN-ORBIT POTENTIAL NOT INCLUDED IN BOTH ENT. AND EXIT CHANNELS (ALSO FOR L=8)
L = 2
L = 3
L = 4
L = 5
L = 6
L = 7
L = 8
40 MeV
35 MeV
30 MeV
25 MeV
dσ/dΩ (RELATIVE UNITS)
θ_{CM} (deg)

Fig. 11

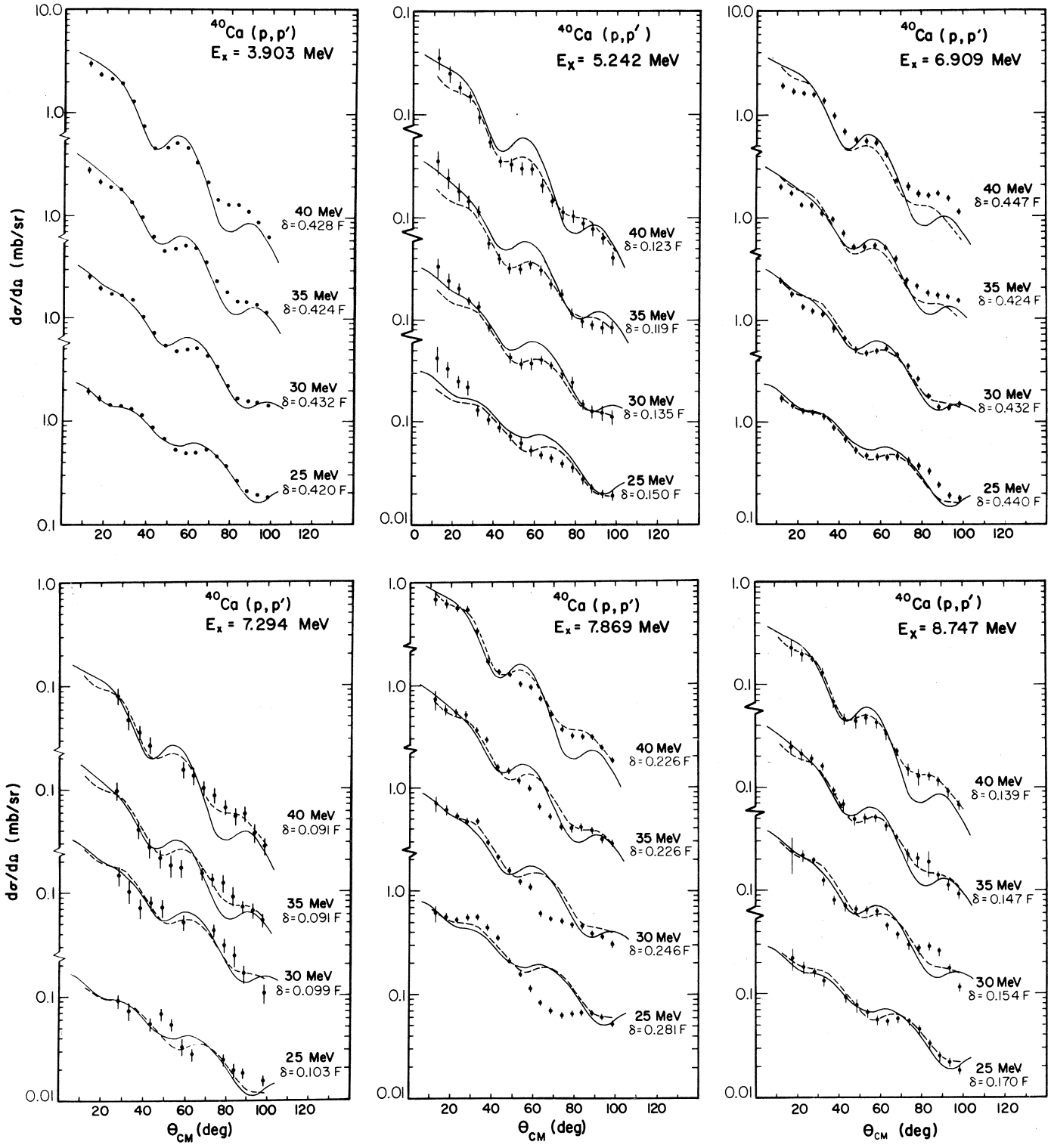
^{40}Ca (p,p')
E_x = 3.903 MeV
40 MeV δ=0.428 F
35 MeV δ=0.424 F
30 MeV δ=0.432 F
25 MeV δ=0.420 F
^{40}Ca (p,p')
E_x = 5.242 MeV
40 MeV δ=0.123 F
35 MeV δ=0.119 F
30 MeV δ=0.135 F
25 MeV δ=0.150 F
^{40}Ca (p,p')
E_x = 6.909 MeV
40 MeV δ=0.447 F
35 MeV δ=0.424 F
30 MeV δ=0.432 F
25 MeV δ=0.440 F
^{40}Ca (p,p')
E_x = 7.294 MeV
40 MeV δ=0.091 F
35 MeV δ=0.091 F
30 MeV δ=0.099 F
25 MeV δ=0.103 F
^{40}Ca (p,p')
E_x = 7.869 MeV
40 MeV δ=0.226 F
35 MeV δ=0.226 F
30 MeV δ=0.246 F
25 MeV δ=0.281 F
^{40}Ca (p,p')
E_x = 8.747 MeV
40 MeV δ=0.139 F
35 MeV δ=0.147 F
30 MeV δ=0.154 F
25 MeV δ=0.170 F
dσ/dΩ (mb/sr)
θ_{CM} (deg)

Fig. 12

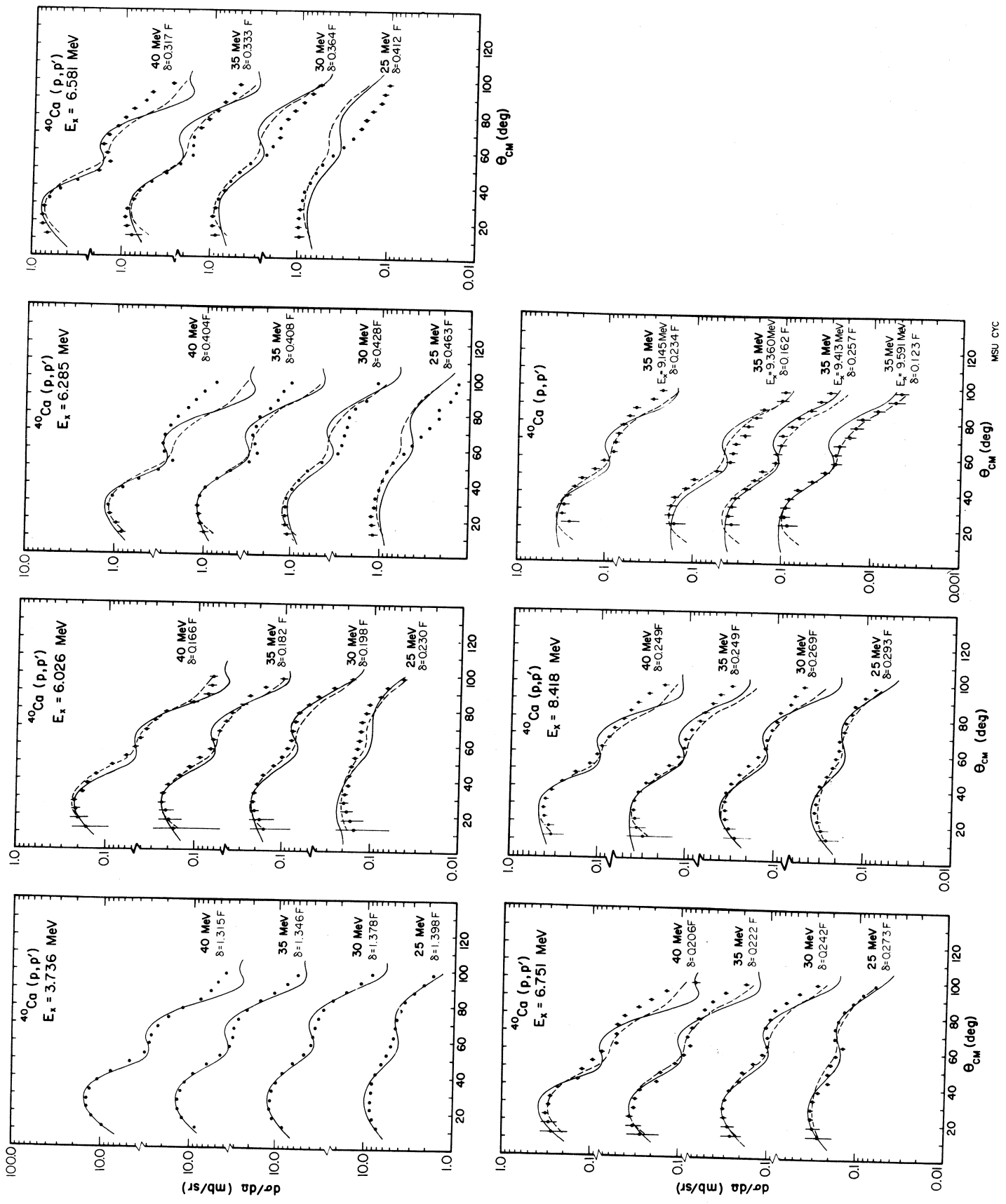
40Ca (p,p')
Ex = 3.736 MeV
40 MeV δ=1.315 F
35 MeV δ=1.346 F
30 MeV δ=1.378 F
25 MeV δ=1.398 F
40Ca (p,p')
Ex = 6.026 MeV
40 MeV δ=0.166 F
35 MeV δ=0.182 F
30 MeV δ=0.198 F
25 MeV δ=0.230 F
40Ca (p,p')
Ex = 6.285 MeV
40 MeV δ=0.404 F
35 MeV δ=0.408 F
30 MeV δ=0.428 F
25 MeV δ=0.463 F
40Ca (p,p')
Ex = 6.581 MeV
40 MeV δ=0.317 F
35 MeV δ=0.333 F
30 MeV δ=0.364 F
25 MeV δ=0.412 F
40Ca (p,p')
Ex = 6.751 MeV
40 MeV δ=0.206 F
35 MeV δ=0.222 F
30 MeV δ=0.242 F
25 MeV δ=0.273 F
40Ca (p,p')
Ex = 8.418 MeV
40 MeV δ=0.249 F
35 MeV δ=0.249 F
30 MeV δ=0.269 F
25 MeV δ=0.293 F
40Ca (p,p')
35 MeV Ex = 9.145 MeV δ=0.234 F
35 MeV Ex = 9.360 MeV δ=0.162 F
35 MeV Ex = 9.413 MeV δ=0.257 F
35 MeV Ex = 9.591 MeV δ=0.123 F
dσ/dΩ (mb/sr)
θCM (deg)
MSU CYC

Fig. 13

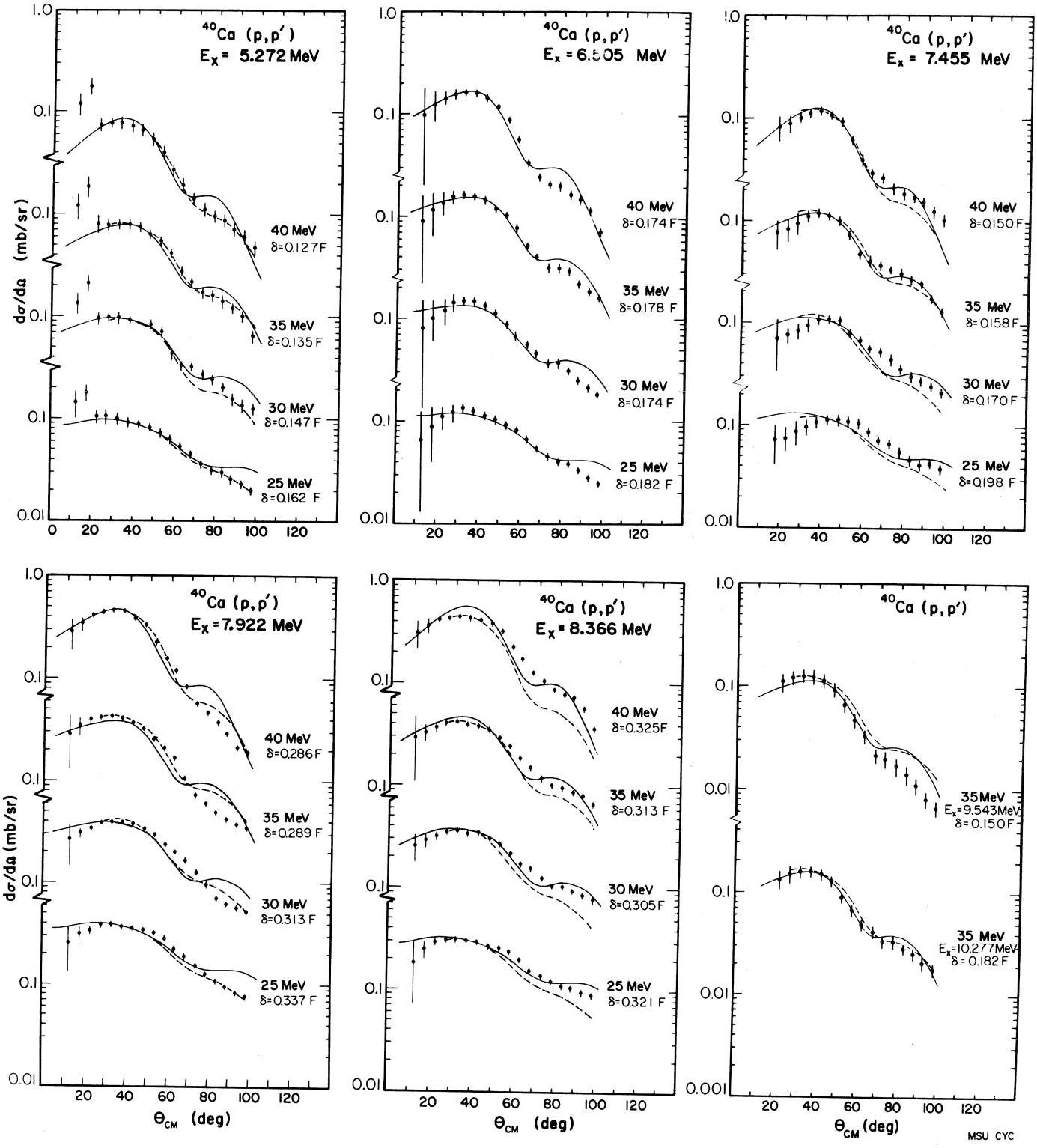
40Ca (p,p')
Ex = 5.272 MeV
40 MeV δ=0.127F
35 MeV δ=0.135F
30 MeV δ=0.147F
25 MeV δ=0.162 F
40Ca (p,p')
Ex = 6.505 MeV
40 MeV δ=0.174F
35 MeV δ=0.178 F
30 MeV δ=0.174 F
25 MeV δ=0.182 F
40Ca (p,p')
Ex = 7.455 MeV
40 MeV δ=0.150F
35 MeV δ=0.158F
30 MeV δ=0.170F
25 MeV δ=0.198 F
40Ca (p,p')
Ex = 7.922 MeV
40 MeV δ=0.286F
35 MeV δ=0.289 F
30 MeV δ=0.313 F
25 MeV δ=0.337 F
40Ca (p,p')
Ex = 8.366 MeV
40 MeV δ=0.325F
35 MeV δ=0.313 F
30 MeV δ=0.305F
25 MeV δ=0.321 F
40Ca (p,p')
35MeV Ex=9.543MeV δ=0.150F
35 MeV Ex=10.277MeV δ=0.182F
dσ/dΩ (mb/sr)
θCM (deg)
MSU CYC

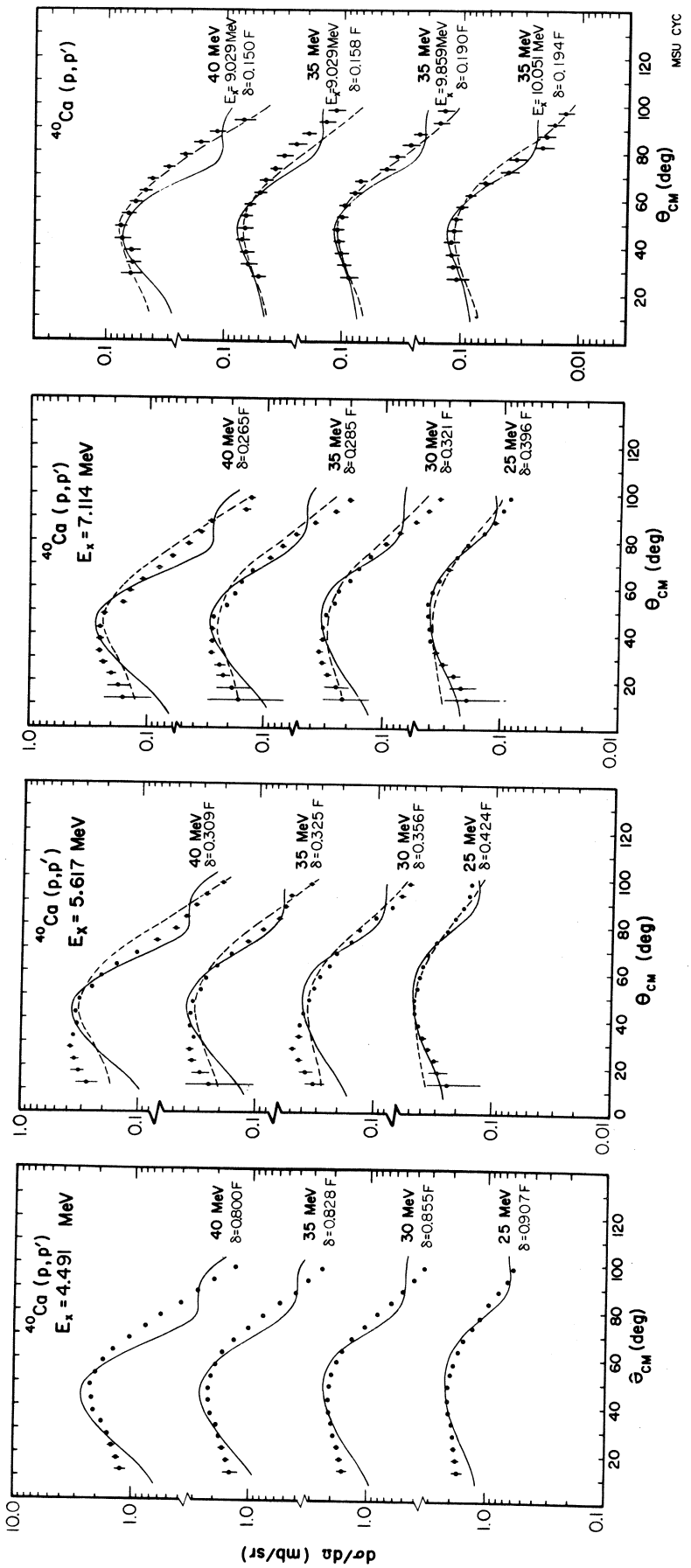
dσ/dΩ (mb/sr)
40Ca (p,p')
Ex = 4.491 MeV
40 MeV δ=0.800F
35 MeV δ=0.828 F
30 MeV δ=0.855F
25 MeV δ=0.907 F
θCM (deg)
40Ca (p,p')
Ex = 5.617 MeV
40 MeV δ=0.309F
35 MeV δ=0.325 F
30 MeV δ=0.356F
25 MeV δ=0.424F
θCM (deg)
40Ca (p,p')
Ex = 7.114 MeV
40 MeV δ=0.265F
35 MeV δ=0.285 F
30 MeV δ=0.321 F
25 MeV δ=0.396 F
θCM (deg)
40Ca (p,p')
40 MeV Ex= 9.029MeV δ=0.150 F
35 MeV Ex=9.029MeV δ=0.158 F
35 MeV Ex=9.859MeV δ=0.190F
35 MeV Ex= 10.051 MeV δ=0.194 F
θCM (deg)
MSU CYC

Fig. 14

Fig. 15

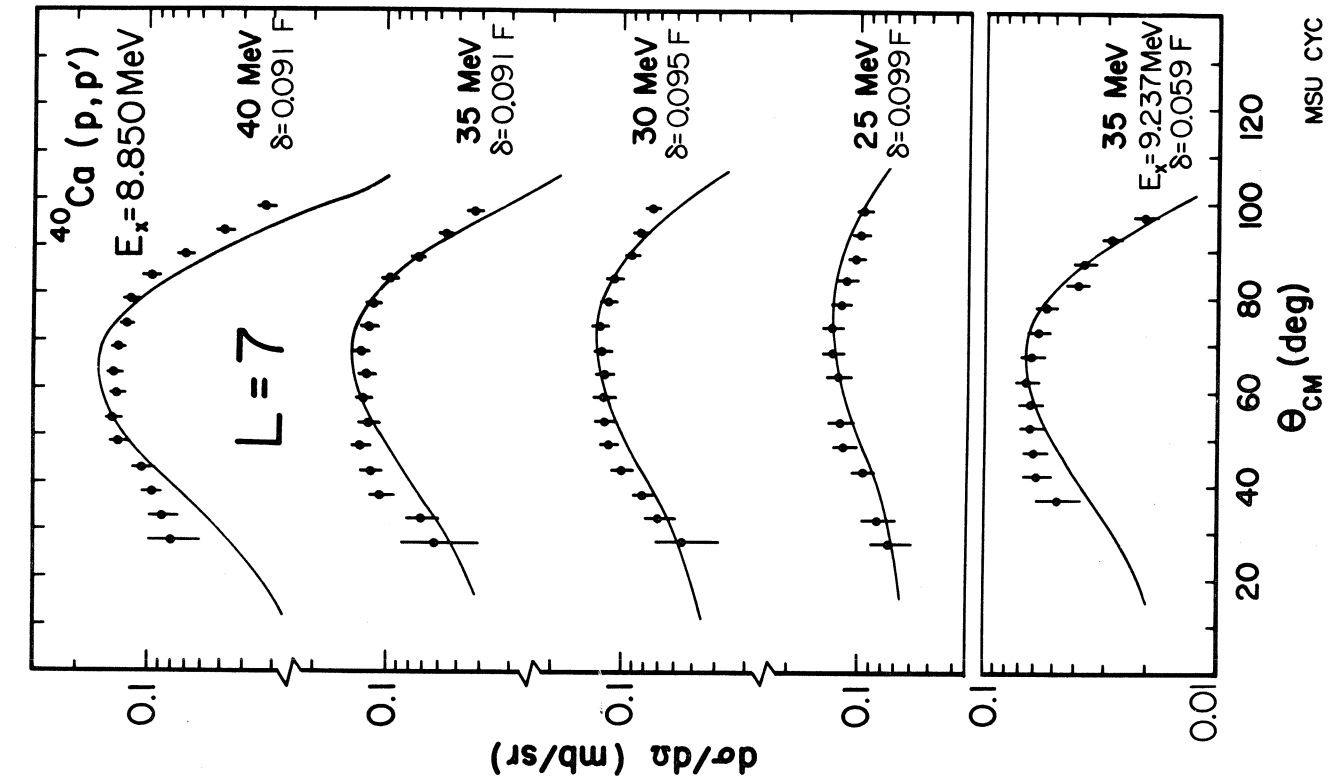
^{40}Ca (p,p')
L=7
E_x=8.850MeV
40 MeV
δ=0.091 F
35 MeV
δ=0.091 F
30 MeV
δ=0.095 F
25 MeV
δ=0.099F
35 MeV
E_x=9.237MeV
δ=0.059 F
dσ/dΩ (mb/sr)
θ_{CM} (deg)
MSU CYC

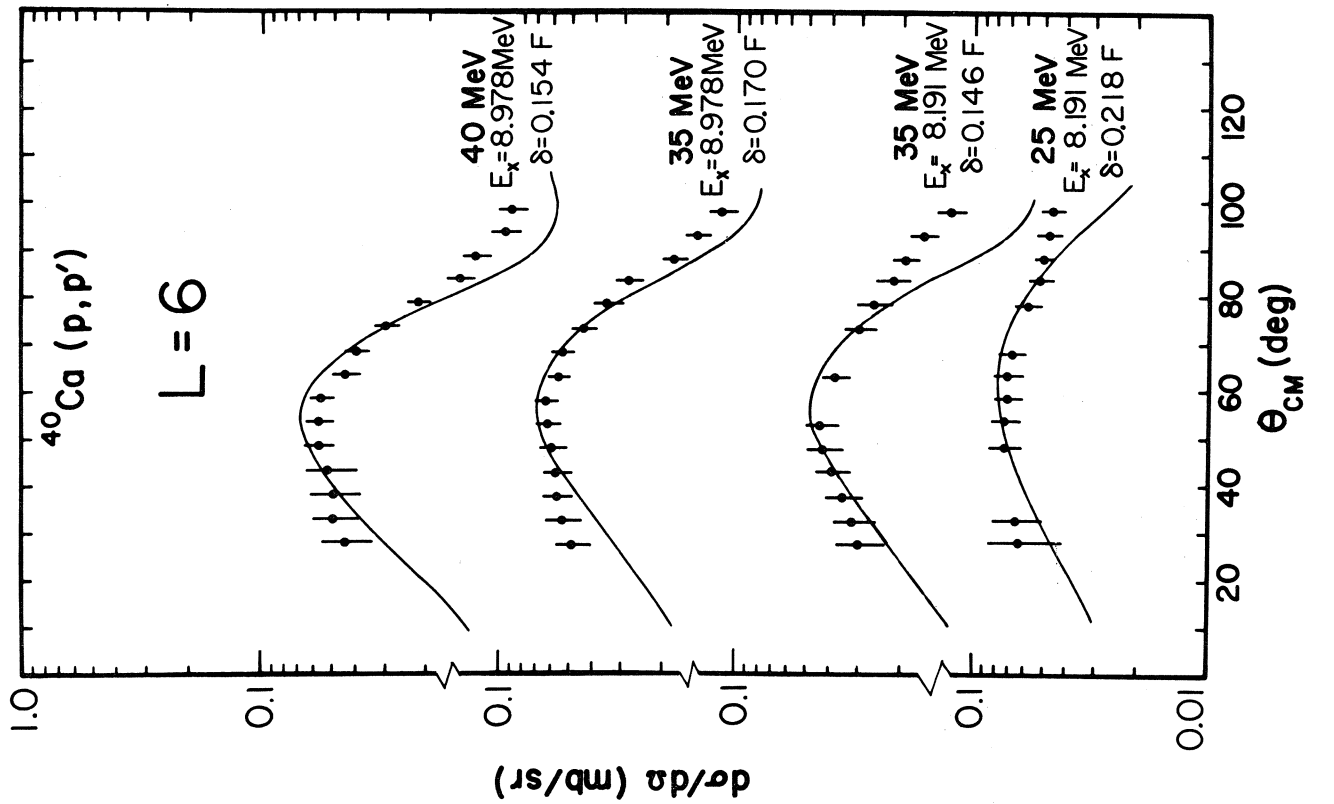
^{40}Ca (p,p')
L=6
40 MeV
E_x=8.978MeV
δ=0.154 F
35 MeV
E_x=8.978MeV
δ=0.170 F
35 MeV
E_x= 8.191 MeV
δ=0.146 F
25 MeV
E_x= 8.191 MeV
δ=0.218 F
dσ/dΩ (mb/sr)
θ_{CM} (deg)

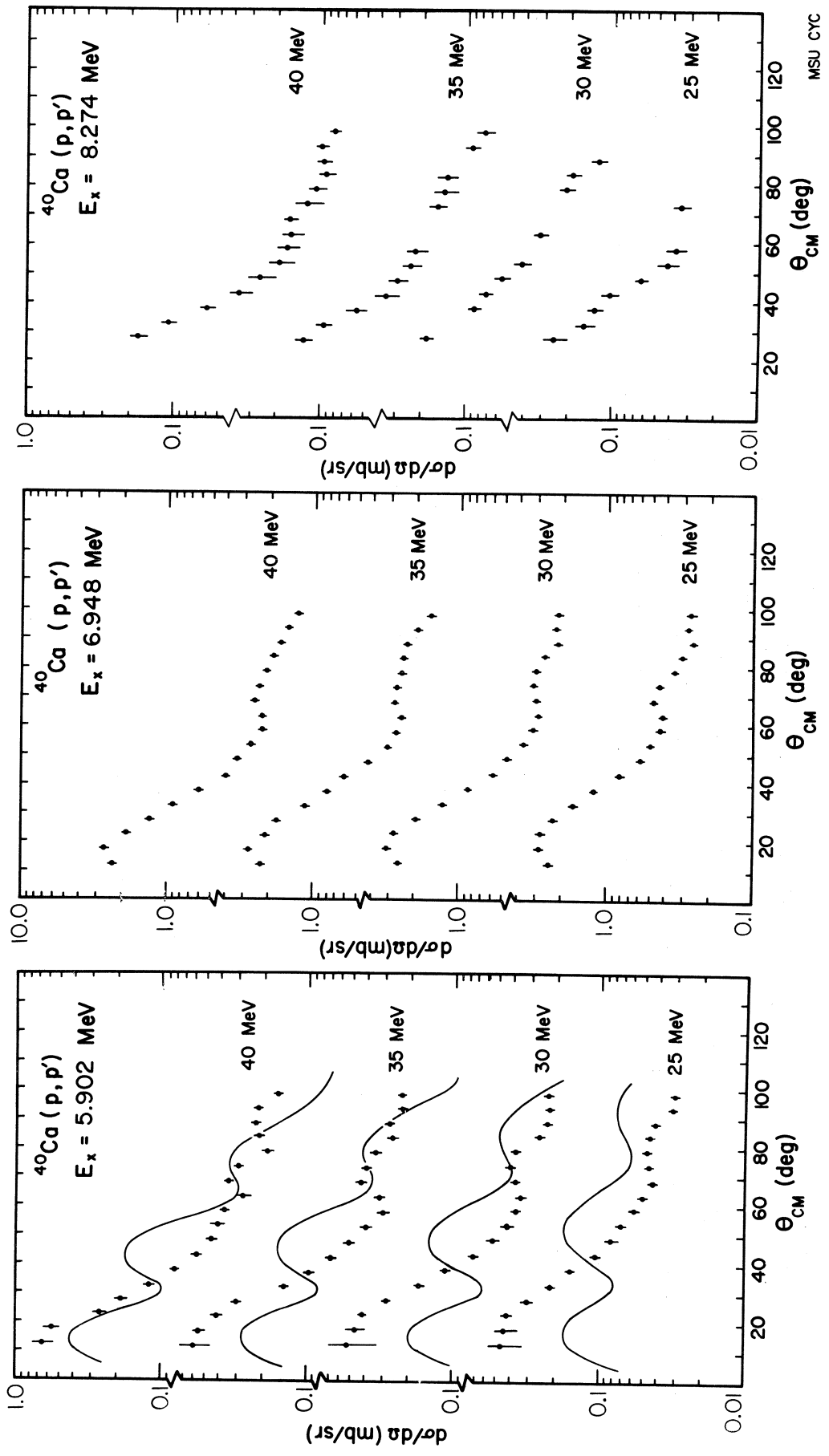
^{40}Ca (p,p')
E_x = 5.902 MeV
^{40}Ca (p,p')
E_x = 6.948 MeV
^{40}Ca (p,p')
E_x = 8.274 MeV
40 MeV
35 MeV
30 MeV
25 MeV
dσ/dΩ (mb/sr)
θ_{CM} (deg)
MSU CYC

Fig. 16

Fig. 17

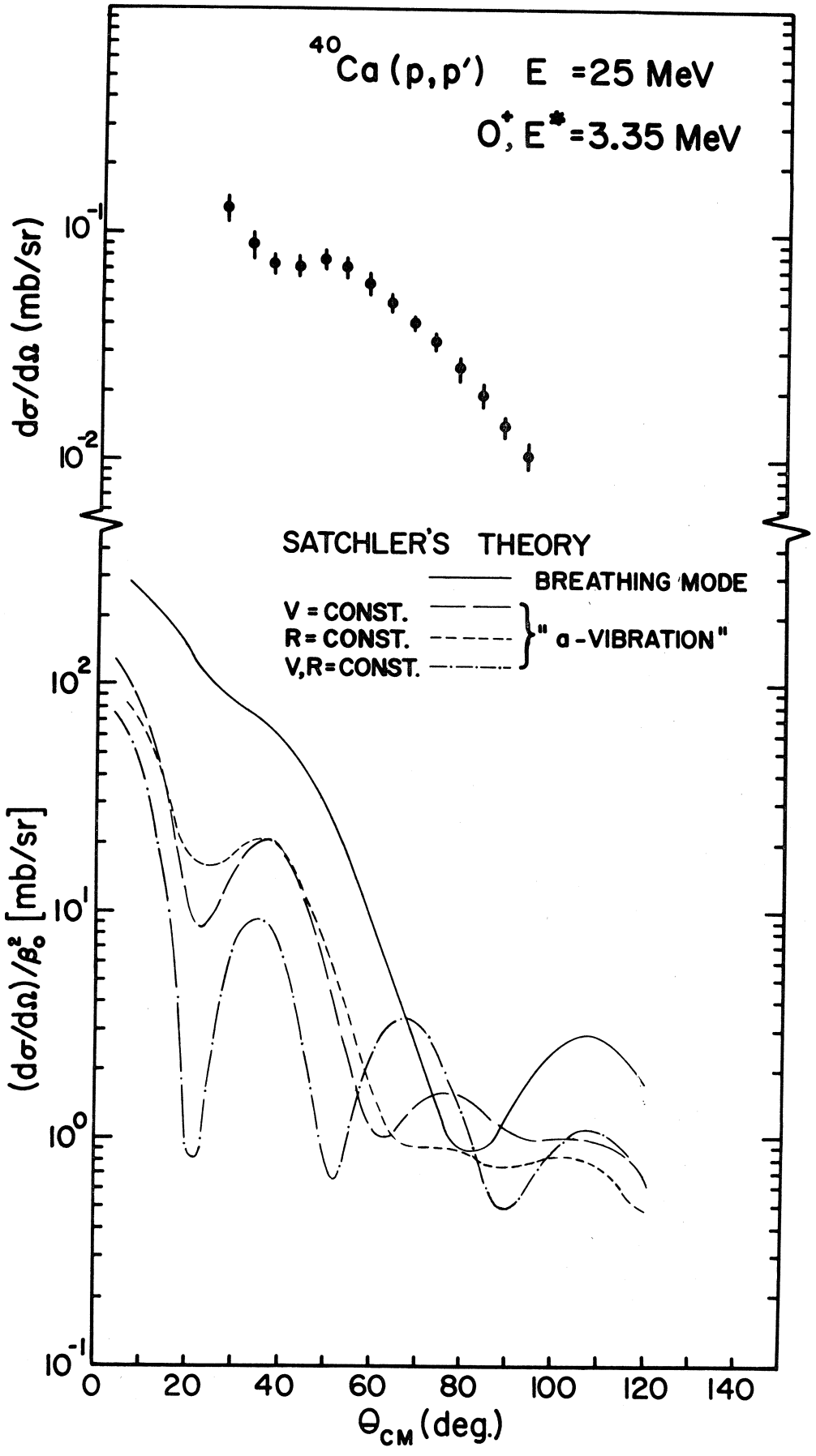
^{40}Ca (p, p′) E =25 MeV
0^{+}, E*=3.35 MeV
dσ/dΩ (mb/sr)
SATCHLER'S THEORY
BREATHING MODE
V = CONST.
R = CONST.
V,R=CONST.
" α-VIBRATION"
(dσ/dΩ)/β$_0^2$ [mb/sr]
θ$_{CM}$ (deg.)

Fig. 18

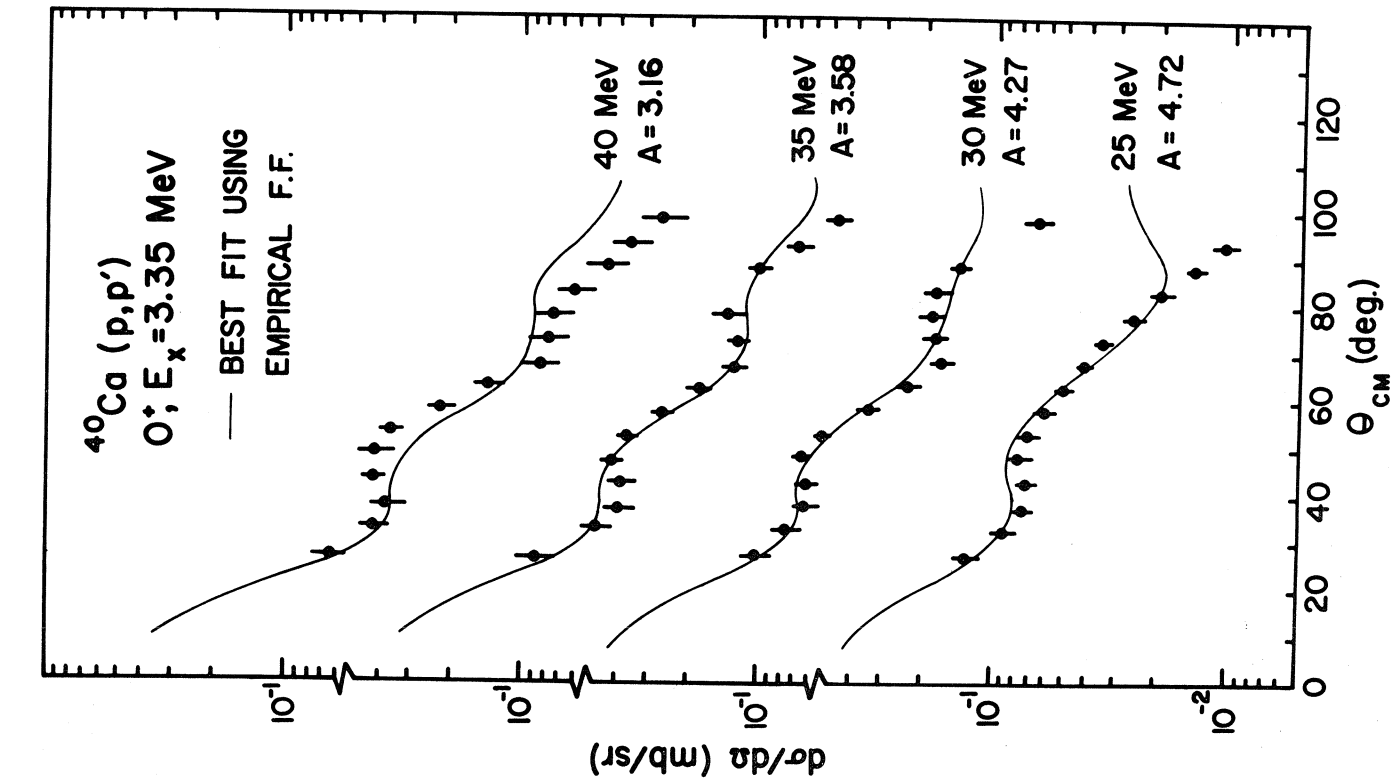
^{40}Ca (p,p')
0^+; E_x=3.35 MeV
— BEST FIT USING
EMPIRICAL F.F.
40 MeV
A = 3.16
35 MeV
A = 3.58
30 MeV
A = 4.27
25 MeV
A = 4.72
dσ/dΩ (mb/sr)
Θ_{cm} (deg.)

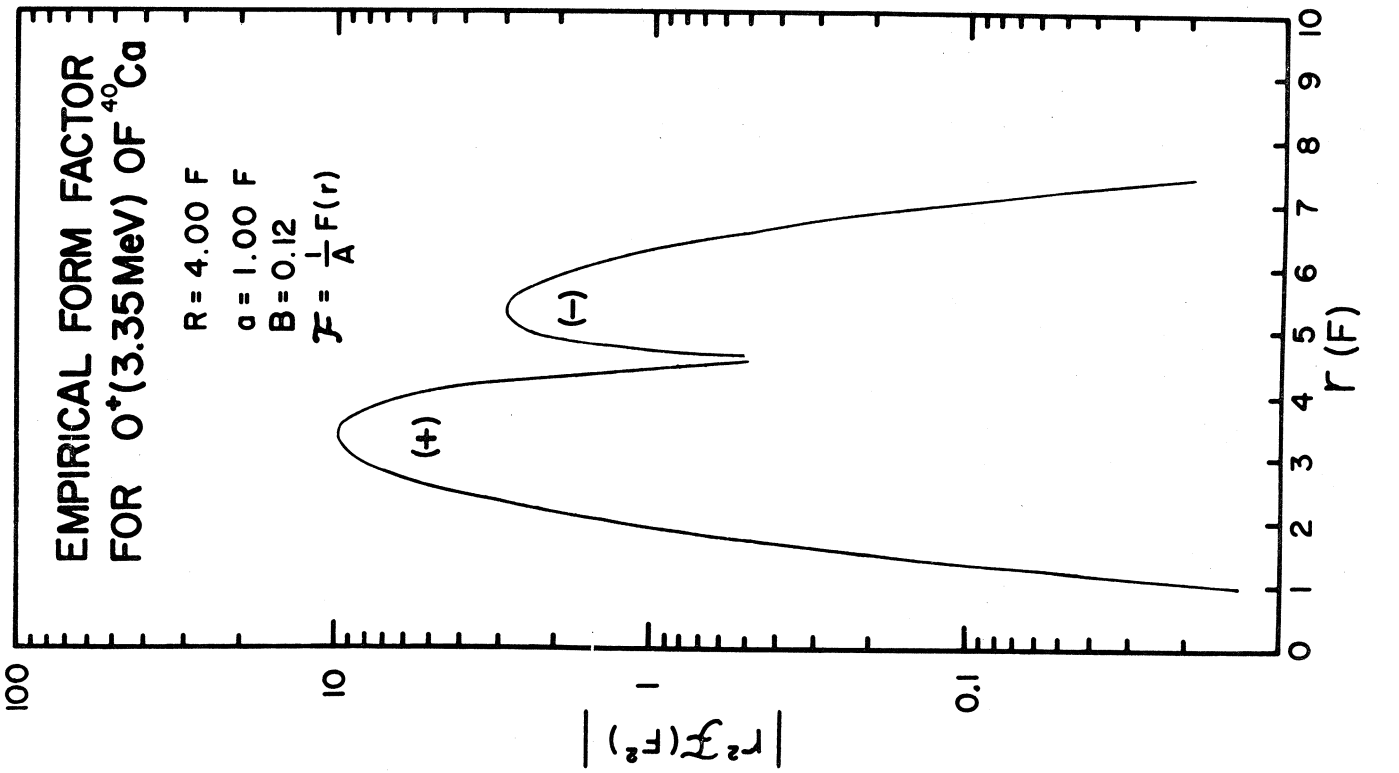
EMPIRICAL FORM FACTOR
FOR 0^+(3.35MeV) OF ^{40}Ca
R = 4.00 F
a = 1.00 F
B = 0.12
$\mathcal{F} = \frac{1}{A} F(r)$
(+)
(−)
$|r^2\mathcal{F}(F^2)|$
r (F)

Fig. 19

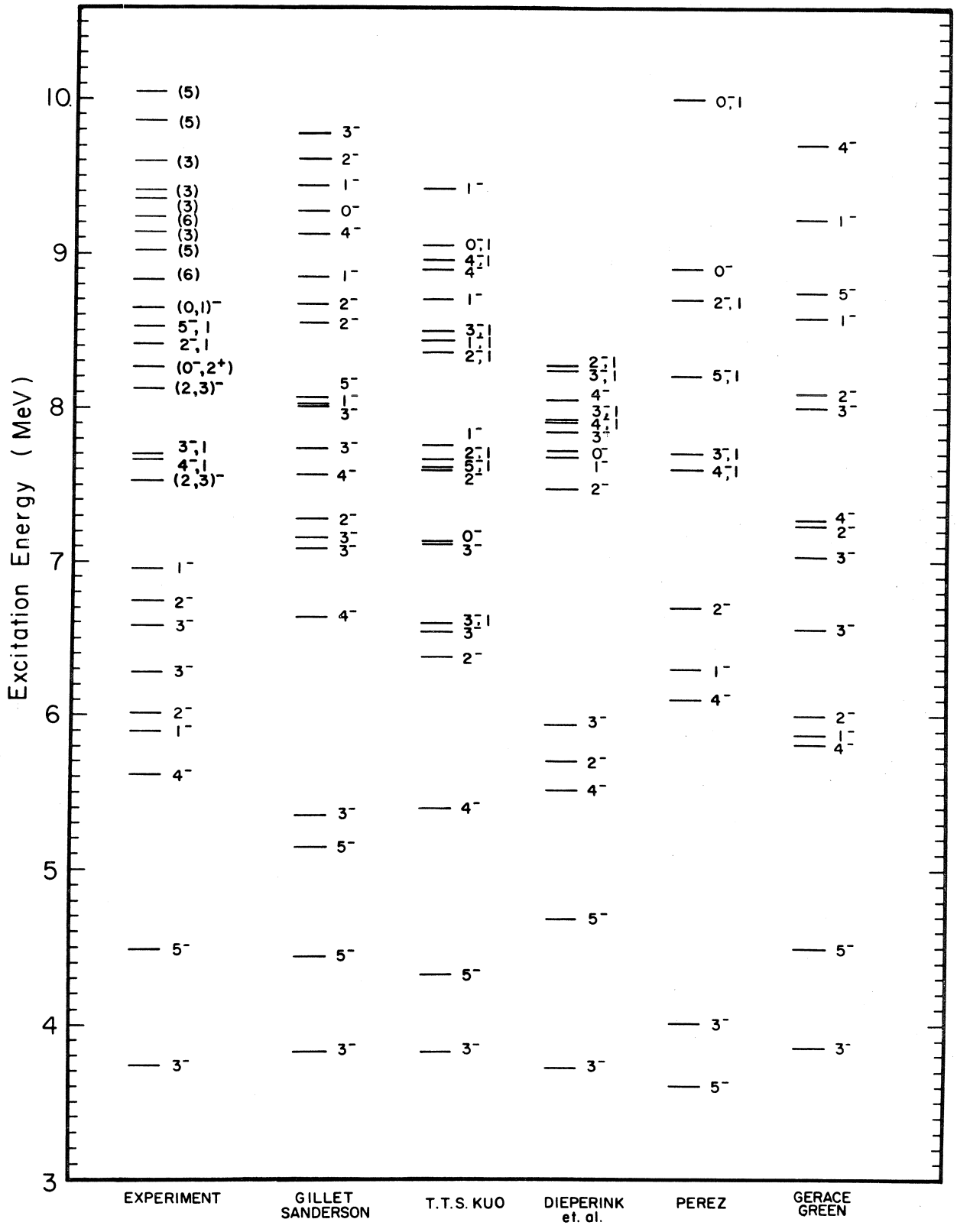
Excitation Energy (MeV)
10
9
8
7
6
5
4
3
EXPERIMENT
GILLET SANDERSON
T.T.S. KUO
DIEPERINK et. al.
PEREZ
GERACE GREEN

Fig. 20

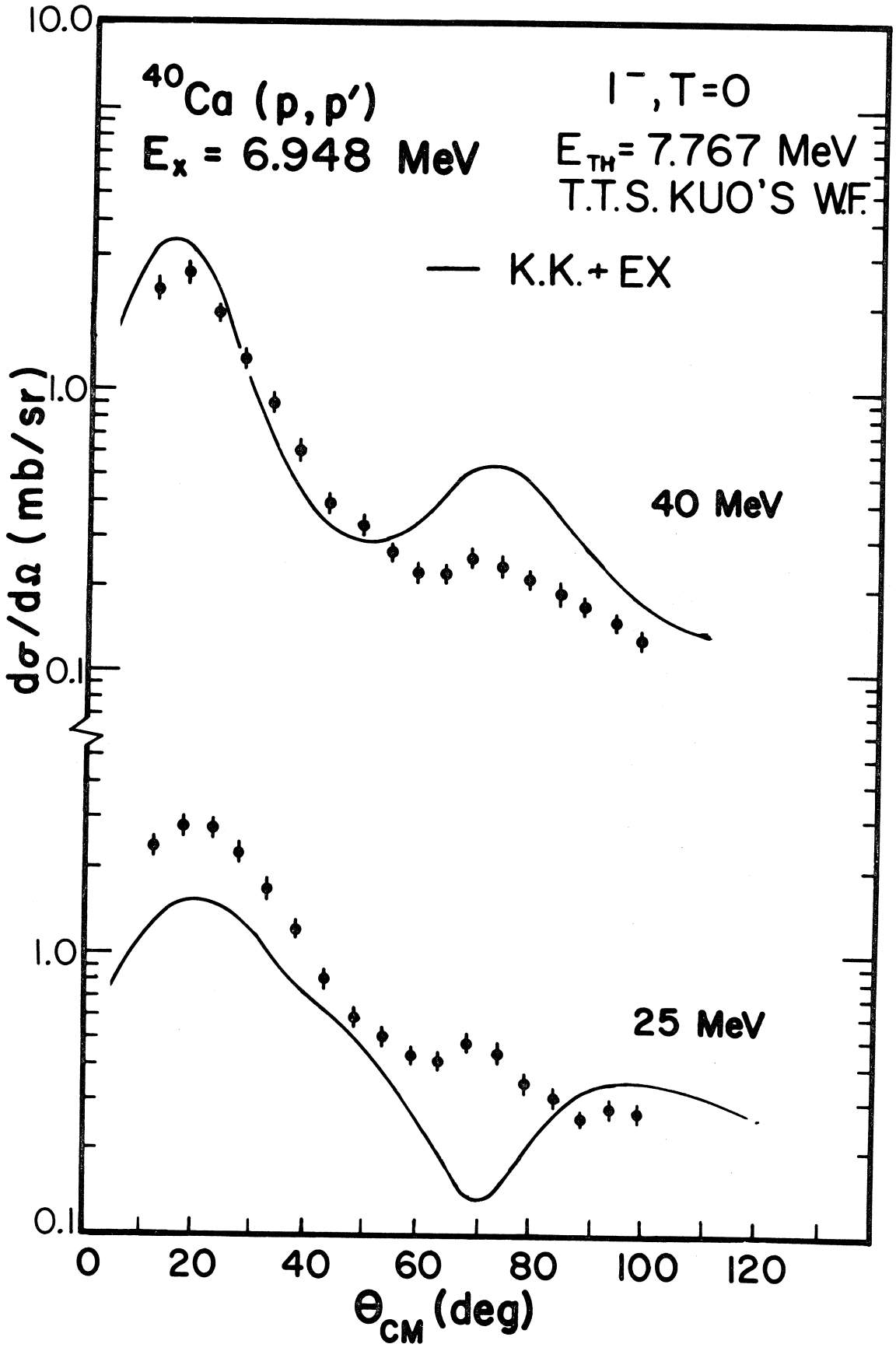
10.0
1.0
0.1
1.0
0.1
^{40}Ca (p, p′)
E_x = 6.948 MeV
1⁻, T=0
E_{TH}= 7.767 MeV
T.T.S. KUO'S W.F.
— K.K.+EX
40 MeV
25 MeV
dσ/dΩ (mb/sr)
0
20
40
60
80
100
120
Θ_{CM} (deg)

Fig. 21

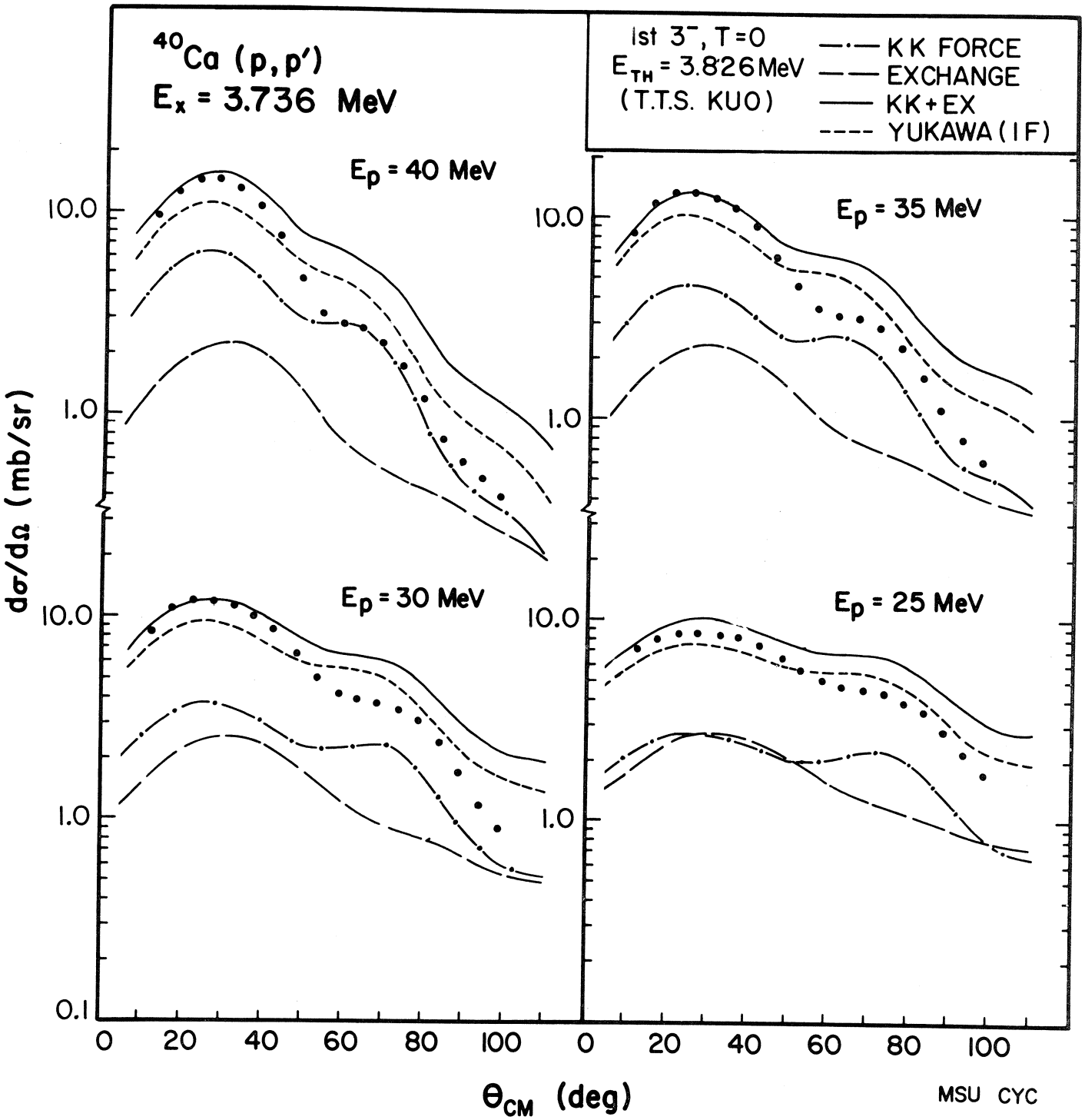
^{40}Ca (p, p')
E_x = 3.736 MeV
1st 3⁻, T=0
E_{TH} = 3.826 MeV
(T.T.S. KUO)
KK FORCE
EXCHANGE
KK + EX
YUKAWA (1F)
E_p = 40 MeV
E_p = 35 MeV
E_p = 30 MeV
E_p = 25 MeV
dσ/dΩ (mb/sr)
10.0
1.0
0.1
0
20
40
60
80
100
Θ_{CM} (deg)
MSU CYC

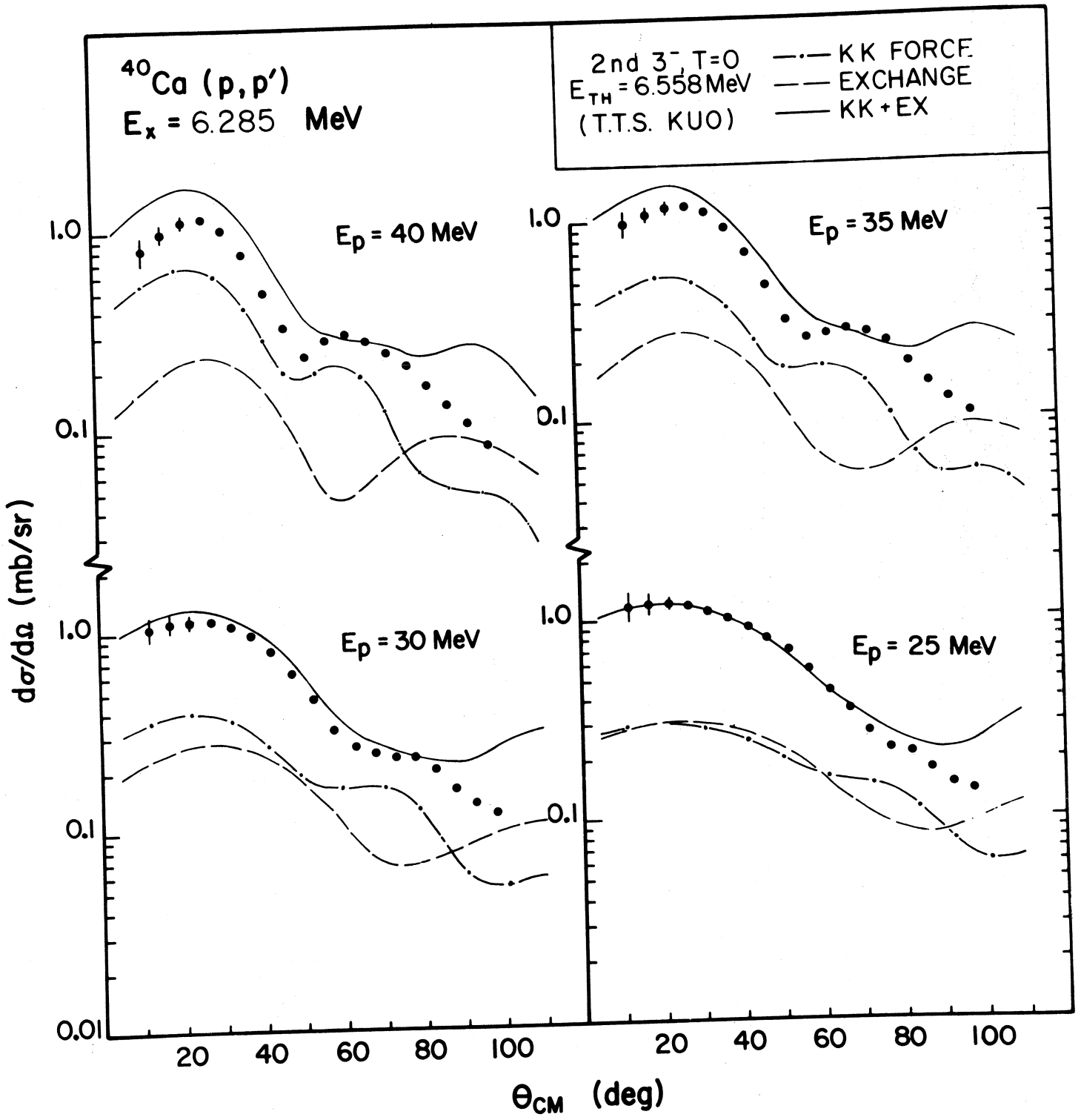
^{40}Ca (p, p')
E_x = 6.285 MeV
2nd 3$^-$, T=0
E_{TH} = 6.558 MeV
(T.T.S. KUO)
KK FORCE
EXCHANGE
KK + EX
E_p = 40 MeV
E_p = 35 MeV
E_p = 30 MeV
E_p = 25 MeV
dσ/dΩ (mb/sr)
Θ_{CM} (deg)
1.0
0.1
0.01
20
40
60
80
100

Fig. 23

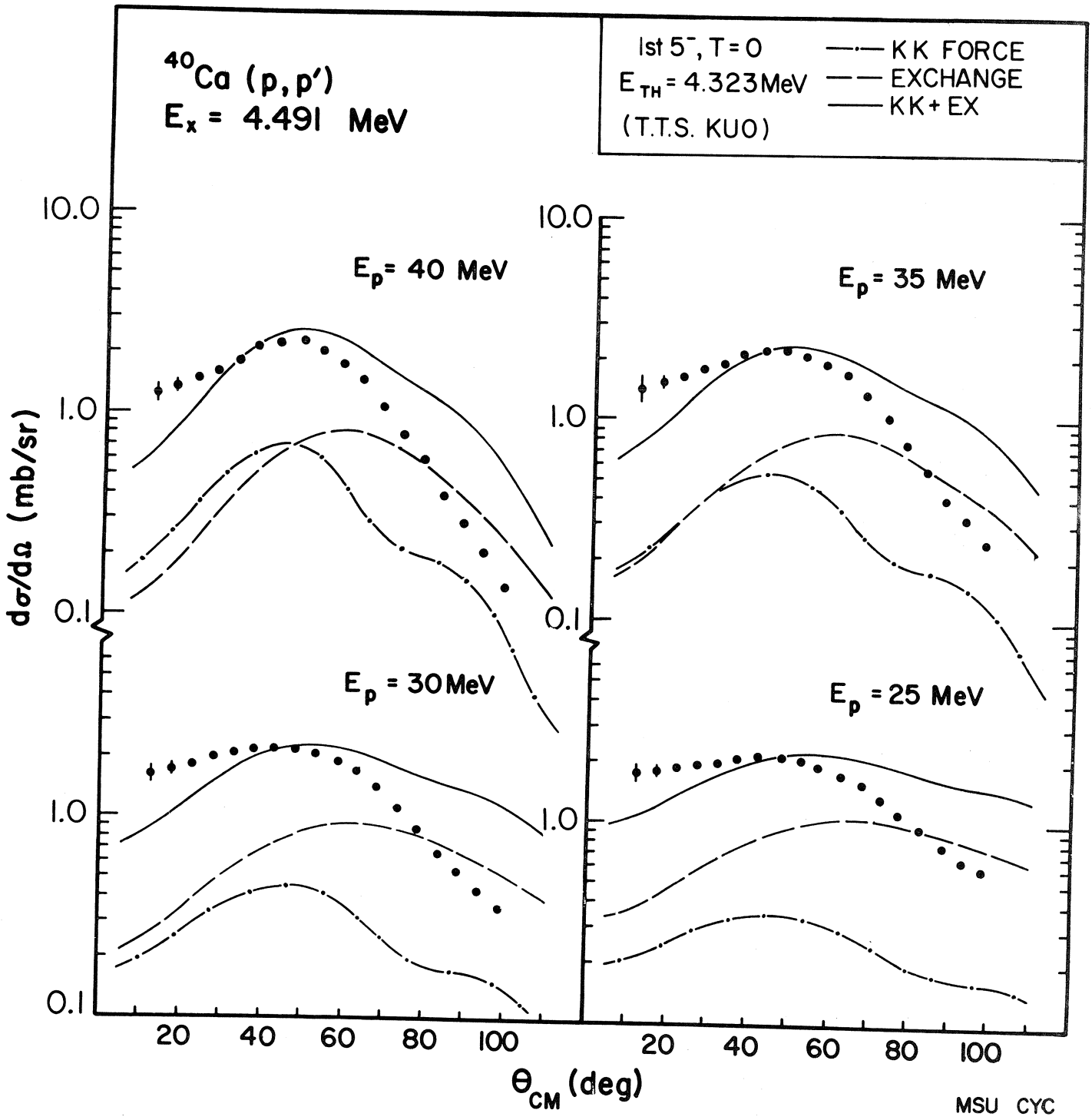
^{40}Ca (p, p')
E_x = 4.491 MeV
1st 5$^-$, T = 0
E_{TH} = 4.323MeV
(T.T.S. KUO)
KK FORCE
EXCHANGE
KK + EX
E_p = 40 MeV
E_p = 35 MeV
E_p = 30MeV
E_p = 25 MeV
10.0
1.0
0.1
dσ/dΩ (mb/sr)
20
40
60
80
100
θ_{CM} (deg)
MSU CYC

Fig. 24

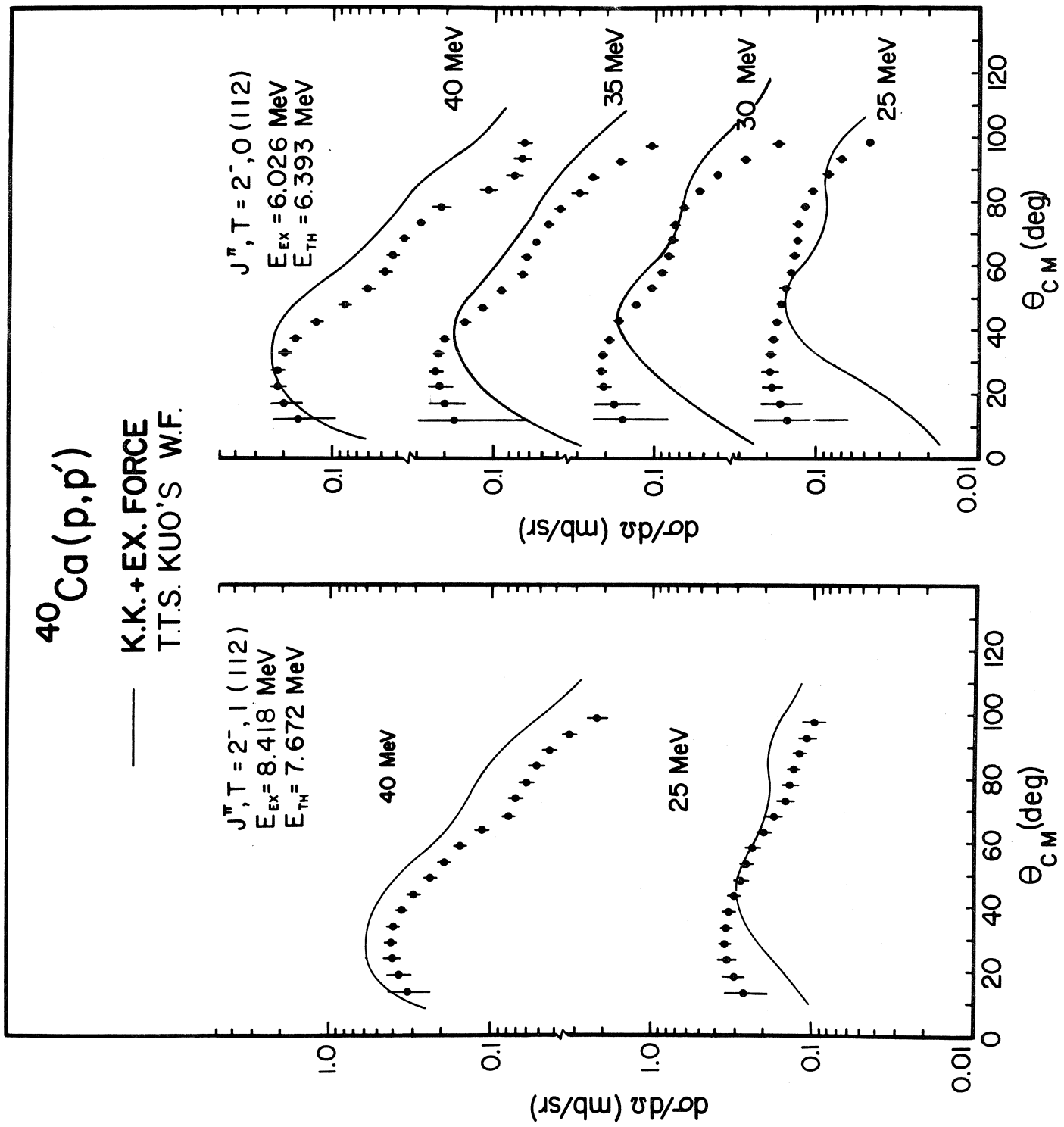
^{40}Ca(p,p')
K.K.+EX. FORCE
T.T.S. KUO'S W.F.
$J^\pi, T = 2^-, 1\ (112)$
$E_{EX} = 8.418$ MeV
$E_{TH} = 7.672$ MeV
40 MeV
25 MeV
$J^\pi, T = 2^-, 0\ (112)$
$E_{EX} = 6.026$ MeV
$E_{TH} = 6.393$ MeV
40 MeV
35 MeV
30 MeV
25 MeV
dσ/dΩ (mb/sr)
θ_{CM} (deg)

Fig. 25

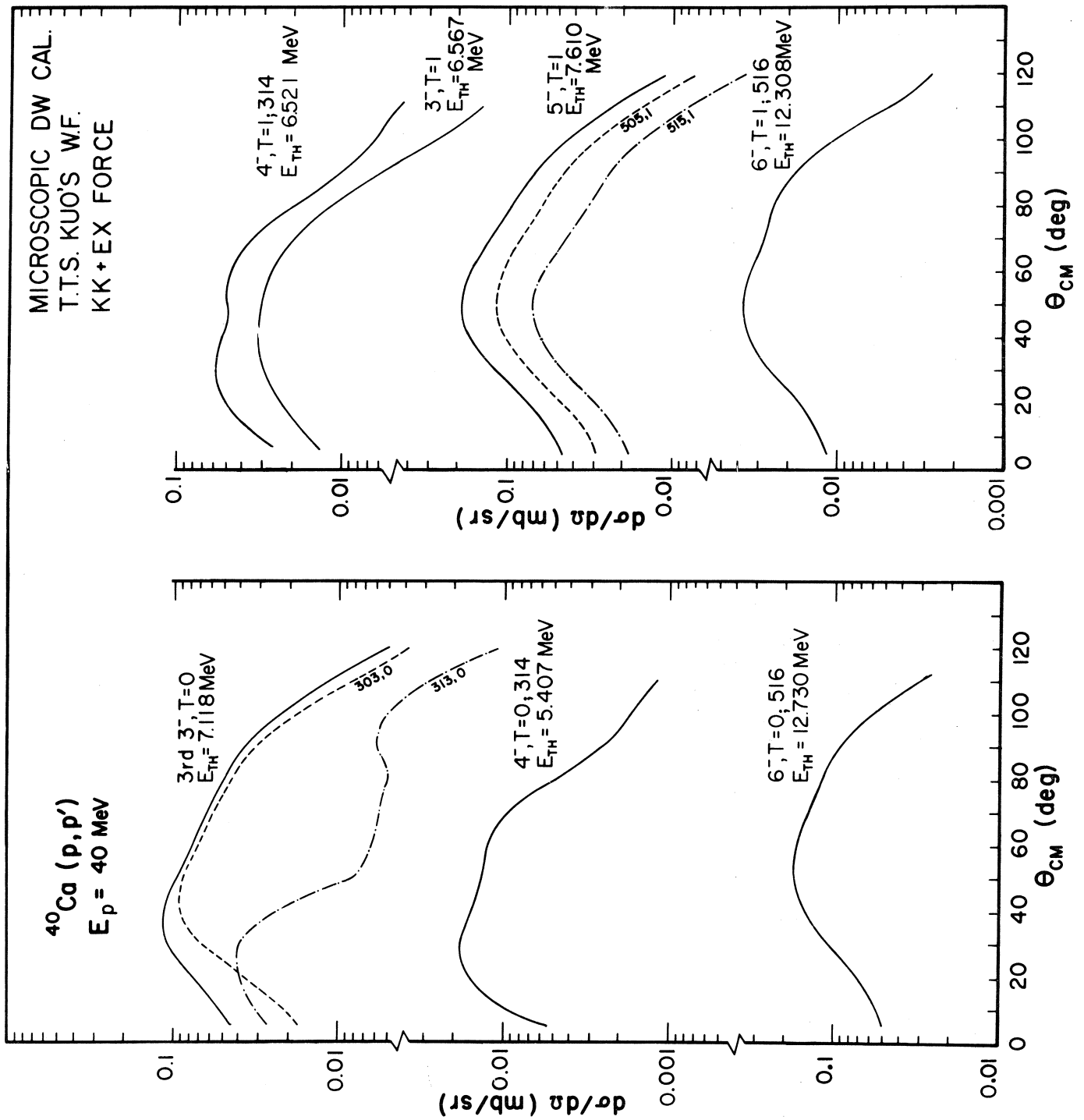
MICROSCOPIC DW CAL.
T.T.S. KUO'S W.F.
K K + EX FORCE
40Ca (p,p')
Ep= 40 MeV
3rd 3⁻ T=0
ETH= 7.118MeV
305,0
313,0
4⁻ T=0; 314
ETH= 5.407 MeV
6⁻ T=0; 516
ETH= 12.730 MeV
4⁻ T=1; 314
ETH= 6.521 MeV
3⁻ T=1
ETH=6.567 MeV
5⁻ T=1
ETH=7.610 MeV
305,1
315,1
6⁻ T=1; 516
ETH=12.308MeV
dσ/dΩ (mb/sr)
θCM (deg)

Fig. 26

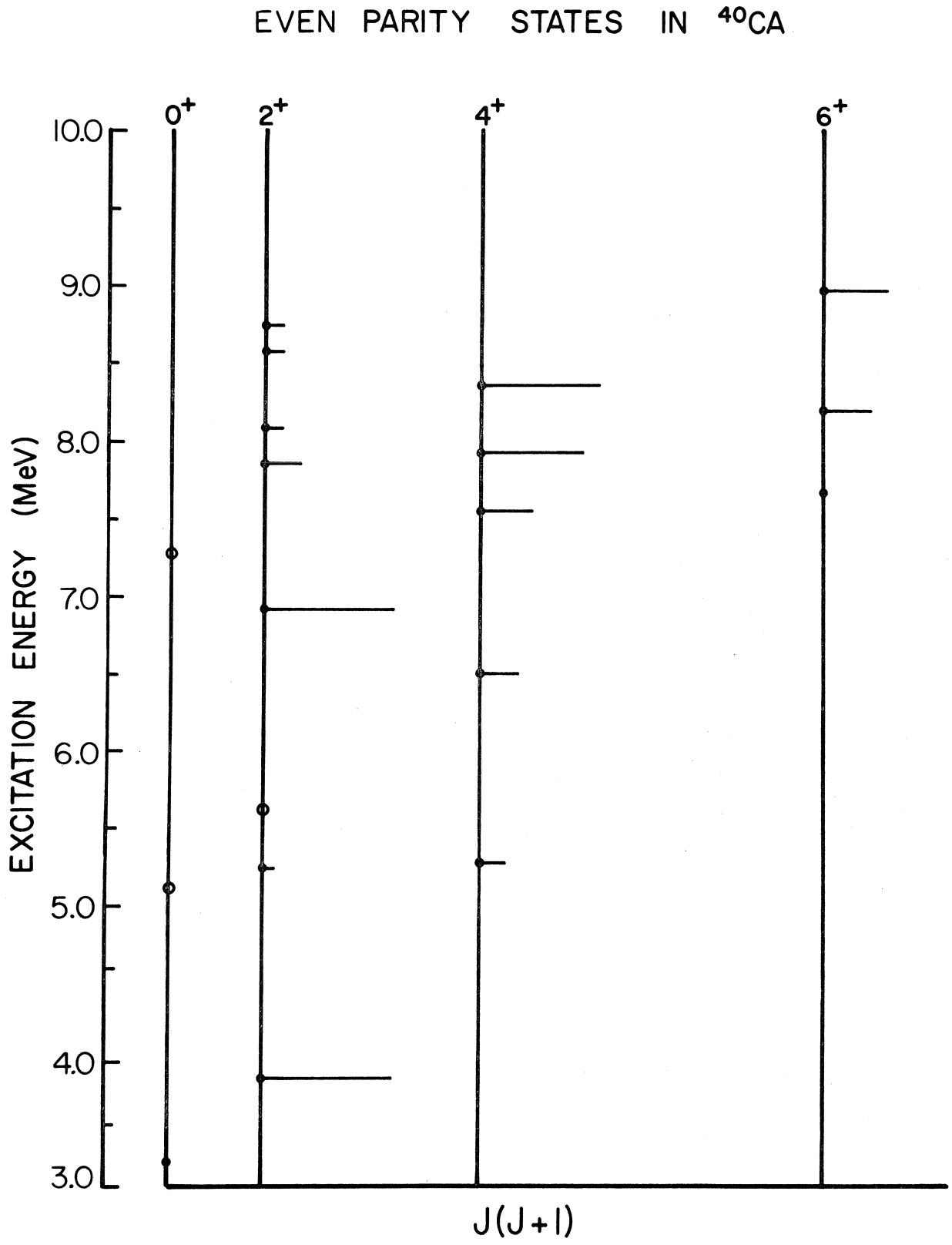
EVEN PARITY STATES IN ^{40}CA
0+
2+
4+
6+
10.0
9.0
8.0
7.0
6.0
5.0
4.0
3.0
EXCITATION ENERGY (MeV)
J(J+1)

Fig. 27

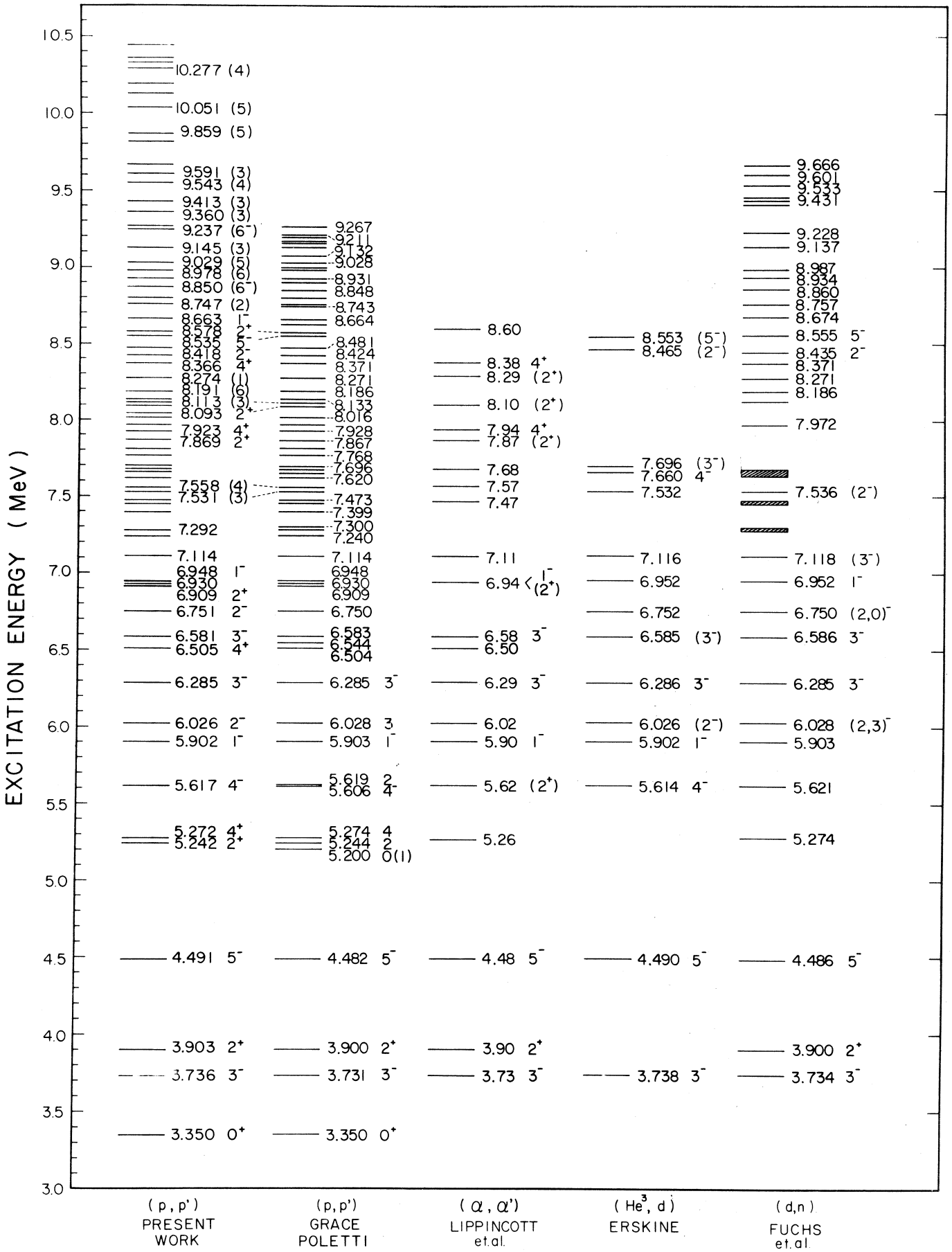
EXCITATION ENERGY (MeV)
10.5
10.0
9.5
9.0
8.5
8.0
7.5
7.0
6.5
6.0
5.5
5.0
4.5
4.0
3.5
3.0
10.277 (4)
10.051 (5)
9.859 (5)
9.591 (3)
9.543 (4)
9.413 (3)
9.360 (3)
9.237 (6⁻)
9.145 (3)
9.029 (5)
8.978 (6)
8.850 (6⁻)
8.747 (2)
8.663 1⁻
8.578 2⁺
8.535 5⁻
8.418 2⁻
8.366 4⁺
8.274 (1)
8.191 (6)
8.113 (3)
8.093 2⁺
7.923 4⁺
7.869 2⁺
7.558 (4)
7.531 (3)
7.292
7.114
6.948 1⁻
6.930
6.909 2⁺
6.751 2⁻
6.581 3⁻
6.505 4⁺
6.285 3⁻
6.026 2⁻
5.902 1⁻
5.617 4⁻
5.272 4⁺
5.242 2⁺
4.491 5⁻
3.903 2⁺
3.736 3⁻
3.350 0⁺
9.267
9.211
9.132
9.028
8.931
8.848
8.743
8.664
8.481
8.424
8.371
8.271
8.186
8.133
8.016
7.928
7.867
7.768
7.696
7.620
7.473
7.399
7.300
7.240
7.114
6.948
6.930
6.909
6.750
6.583
6.544
6.504
6.285 3⁻
6.028 3
5.903 1⁻
5.619 2
5.606 4⁻
5.274 4
5.244 2
5.200 0(1)
4.482 5⁻
3.900 2⁺
3.731 3⁻
3.350 0⁺
8.60
8.38 4⁺
8.29 (2⁺)
8.10 (2⁺)
7.94 4⁺
7.87 (2⁺)
7.68
7.57
7.47
7.11
6.94 1⁻ (2⁺)
6.58 3⁻
6.50
6.29 3⁻
6.02
5.90 1⁻
5.62 (2⁺)
5.26
4.48 5⁻
3.90 2⁺
3.73 3⁻
8.553 (5⁻)
8.465 (2⁻)
7.696 (3⁻)
7.660 4⁻
7.532
7.116
6.952
6.752
6.585 (3⁻)
6.286 3⁻
6.026 (2⁻)
5.902 1⁻
5.614 4⁻
4.490 5⁻
3.738 3⁻
9.666
9.601
9.533
9.431
9.228
9.137
8.987
8.934
8.860
8.757
8.674
8.555 5⁻
8.435 2⁻
8.371
8.271
8.186
7.972
7.536 (2⁻)
7.118 (3⁻)
6.952 1⁻
6.750 (2,0)⁻
6.586 3⁻
6.285 3⁻
6.028 (2,3)⁻
5.903
5.621
5.274
4.486 5⁻
3.900 2⁺
3.734 3⁻
(p , p')
PRESENT
WORK
(p, p')
GRACE
POLETTI
(α , α')
LIPPINCOTT
et.al.
(He³ , d)
ERSKINE
(d,n)
FUCHS
et.al.